Assembly techniques for proton exchange membrane fuel cell stack: A literature review

Ke Song [a,b,*], Yimin Wang [a,b], Yuhang Ding [a,b], Hongjie Xu [a,b], Philip Mueller-Welt [c], Tobias Stuermlinger [c], Katharina Bause [c], Christopher Ehrmann [d], Hannes W. Weinmann [d], Jens Schaefer [d], Juergen Fleischer [d], Kai Zhu [e], Florian Weihard [e], Matthias Trostmann [f], Matthias Schwartze [f], Albert Albers [c]

[a] School of Automotive Studies, Tongji University, Shanghai, 201804, China
[b] National Fuel Cell Vehicle and Powertrain System Engineering Research Center, Tongji University, Shanghai, 201804, China
[c] IPEK Institute of Product Engineering Karlsruhe, Karlsruhe Institute of Technology (KIT), 76131, Karlsruhe, Germany
[d] Wbk Institute of Production Science, Karlsruhe Institute of Technology (KIT), 76131, Karlsruhe, Germany
[e] Ruhlamat Automation Technologies (Suzhou) Co., Ltd. Suzhou, 215021, China
[f] Ruhlamat GmbH, 99834, Gerstungen OT Marksuhl, Germany

Keywords:
Proton exchange membrane fuel cell
Assembly technique
Assembly load
Assembly mechanism
Automatic assembly

A B S T R A C T

The assembly of proton exchange membrane fuel cell (PEMFC) is a complex process. The joint action of the assembly load and the working temperature causes an uneven stress distribution among the components and produces a certain degree of deformation. In addition, the assembly process is often related to load transfer, material transfer, energy exchange, multi-phase flow and electrochemical reaction. At present, the manufacturing cost of fuel cells is extremely high, and assembly cost accounts for a large proportion. Assembly techniques with low efficiency and accuracy further increase manufacturing costs. Therefore, there is an urgent need for further research on stack assembly theory and techniques to improve stack assembly efficiency and reduce costs. Based on a survey of the literature, the research status of assembly load, assembly load optimisation, assembly mechanism, and automatic assembly are summarised. Based on comprehensive analyses, this review proposes the development trends of assembly key techniques for fuel cell stacks, and provides a helpful reference for researchers and producers. In the future, the research of assembly technique should pay more attention to the assembly load of fuel cell under on-line conditions and the joint influence of assembly load and other stresses. The assembly mechanism should be designed according to the application scenario of fuel cell and be more convenient to dynamically adjust the assembly load. The review also points out that automation is the development direction of assembly technique. The design, manufacture and assembly of fuel cells need to be better coordinated.

1. Introduction

Energy has always been the driving force for the development of human society and economy, and the basic resource for the survival of human society [1,2]. It is the principal metric to measure a country's comprehensive national strength, the degree of civilisation development, and the national living standard [3,4]. The history of human social progress shows that every breakthrough in energy technology greatly promotes the development of social productivity [5,6]. In the 21st century, the requirements of human society for energy systems are that they be safe, efficient, clean, and economic. These requirements cannot be met by the current combustion engines or technology. The development of energy faces great challenges [7,8]. Energy production and consumption are closely related to global warming and greenhouse effects [9]. More than half of greenhouse gas emissions are caused by the current global energy system [10]. General fossil fuels release a large amount of carbon dioxide after combustion, which aggravates global warming and accelerates the greenhouse effect [11,12]. As a new type of energy carrier and not natural source of energy, hydrogen has many advantages over other energy sources, such as rich reserves, environmental friendliness, wide range of distribution, and high gravimetric

* Corresponding author. School of Automotive Studies, Tongji University, Shanghai, 201804, China.
E-mail address: ke_song@tongji.edu.cn (K. Song).

Abbreviations

PEMFC	Proton exchange membrane fuel cell
MEA	Membrane electrode assembly
BPP	Bipolar plate
EP	End plate
PEM	Proton exchange membrane
CL	Catalyst layer
GDL	Gas diffusion layer
ICR	Interface contact resistance
CR	Contact resistance
MPL	Micro porous layer
PSD	Pore size distribution
PTFE	Polytetrafluoroethylene
NBR	Nitrite butadiene rubber
FEM	Finite element model
ESM	Equivalent stiffness model
RSM	Response surface methodology
CMM	Coordinate measuring machine

energy density [13,14]. Hydrogen can not only be obtained from fossil energy, but it is also a by-product of many industrial and chemical processes [15]. Therefore, hydrogen is considered as an alternative to the next generation of fossil energy.

Hydrogen energy has many uses, one of which is as the fuel of a proton exchange membrane fuel cell (PEMFC). Fuel cells can directly convert the chemical energy in fuel (hydrogen) and an oxidant (air or oxygen) into available electric energy through internal electrochemical reactions [16,17]. The power generation process is environmentally friendly, efficient, and sustainable [18]. The chemical reaction in a fuel cell is not limited by the Carnot cycle, and thus the energy conversion efficiency of the fuel cell is much higher than that of an internal combustion engine [19,20]. In recent years, fuel cell technology has gradually matured, such that fuel cells have been widely used [21]. However, the high cost of manufacturing has always been a challenging problem [22,23].

Fig. 1 shows the structure of a typical PEMFC stack. PEMFCs consist

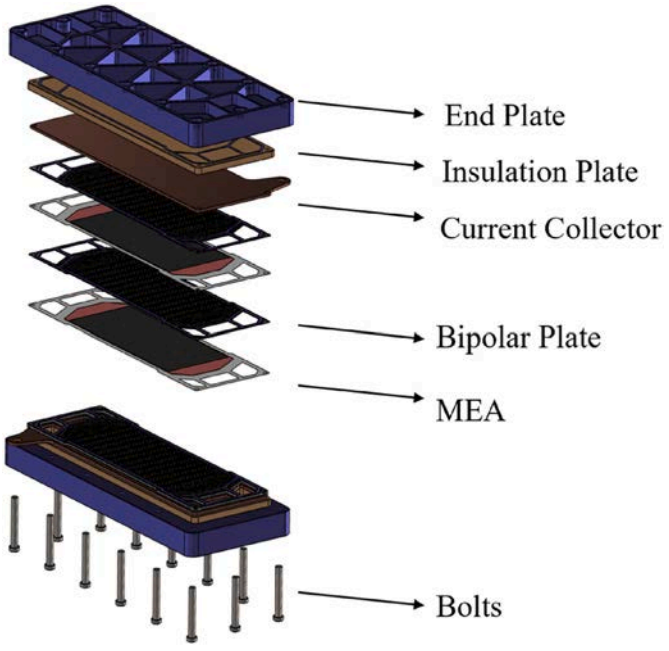

Fig. 1. Composition of PEMFC stack.

of a membrane electrode assembly (MEA), bipolar plate (BPP), end plate (EP), current collector, insulation plate, and sealing gaskets. The basic unit of the fuel cell is composed of an MEA in the middle and a BPP on each side. The MEA is composed of a proton exchange membrane (PEM), a catalyst layer (CL), and a gas diffusion layer (GDL). The structure of the MEA is shown in Fig. 2.

Generally, the output voltage of a single fuel cell is low. In order to improve the power generation capacity of fuel cells, a large number of single fuel cells are assembled into high-power stacks. Fuel cell assembly is a process of stacking many single cells. Finally, different assembly loads are applied to the EP to realise the tight assembly of single fuel cells, as shown in Fig. 3. These components are deformed after being subjected to a certain degree of assembly force, which causes changes in the structure and physical parameters. The changes in these parameters affect the water transfer, reactant transfer, electron transfer, and heat transfer of the fuel cell, and ultimately affect the performance of the fuel cell [24,25]. In this process, the magnitude and distribution of the assembly load is especially important, and the distribution of the assembly load is mainly related to the assembly mechanism. These aspects belong to the category of assembly techniques, which are addressed in this review. In addition, one of the obstacles to fuel cell industrialisation is that the techniques of large-scale manufacturing and assembly are not mature [26,27]. Therefore, it is urgent to achieve theoretical and practical breakthroughs in fuel cell assembly techniques.

In order to optimise the performance of PEMFCs, the first problem of assembly technique research is to determine a reasonable assembly load range. The assembly load has a certain impact on the components and performance of the fuel cell [28,29]. The size and homogeneity of the load and the distribution of the load in the sealing area and flow field are very important. On the one hand, an extremely small assembly load first leads to problems with respect to air tightness. Good air tightness is the first prerequisite to ensure the normal and safe operation of the fuel cell stack in later stages [30,31]. Moreover, it leads to incomplete contact between components, resulting in a sharp rise in the interface contact resistance (ICR). After the input of reaction gas, this leads to a partial open-circuit phenomenon, and the effective voltage of a single cell is reduced [32]. On the other hand, the GDL would be seriously compressed by an excessive assembly load. The GDL is a porous structure. The porosity and permeability decrease sharply after over-extrusion [33]. This not only hinders the diffusion of the reaction gas in the MEA, but also prevents the water generated by the reaction from draining out the fuel cell in time, which also causes the output power of the fuel cell to decrease. The structural strength of the PEM is extremely low, and its structural stress increases rapidly due to over-extrusion. In this case, even if the assembly load were reduced at a later stage, there would be some residual stress in the PEM, which would lead to a serious deterioration in the durability of the PEM [34]. Even if the initial assembly load is reasonable, the interface contact pressure could surge significantly, owing to the swelling of the membrane caused by the temperature rise during fuel cell operation. In addition, the dimensional error (Fig. 4) of the height of the BPP channel may also cause a series of problems such as gas blockage due to excessive local contact pressure. Therefore, the structural and transmission characteristics of the stack are subject to the assembly load. The second problem of the assembly technique is to obtain a uniform assembly load distribution. The fuel cell has a short plate effect; that is, the performance of the fuel cell depends on the worst cell. Uniform pressure distribution can ensure that the electrochemical reaction conditions and sealing conditions of the sealing zone are essentially the same. It is worth pointing out that the distribution of pressure has a significant relationship with the assembly mechanism, which is also one of the problems in the research of assembly techniques. With the increasing level of automation, people try to improve the production efficiency by automatic assembly and avoid possible human errors in the assembly process. Therefore, more and more attention has been paid to the automated assembly of stacks in recent years.

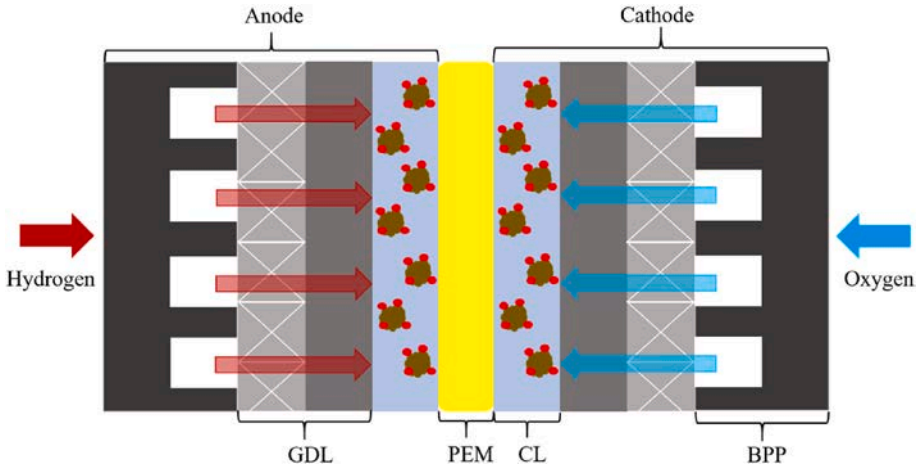

Fig. 2. MEA structure.

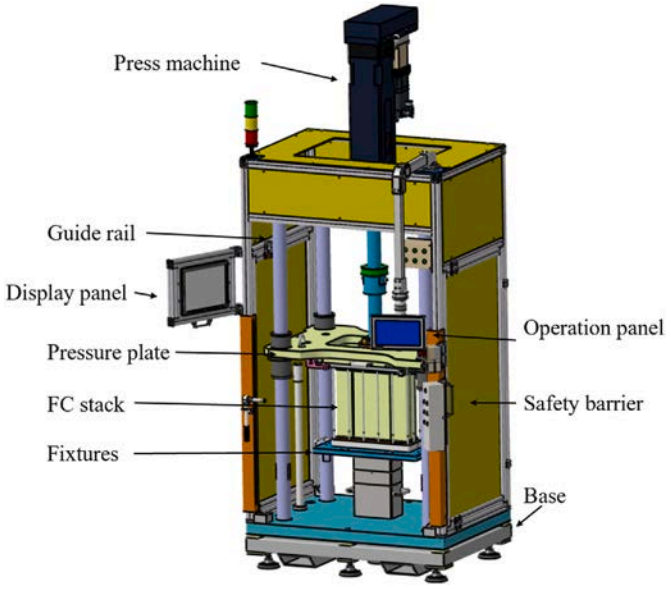

Fig. 3. PEMFC stack assembly (*Ruhlamat Automation Technologies (Suzhou) Co., Ltd)*.

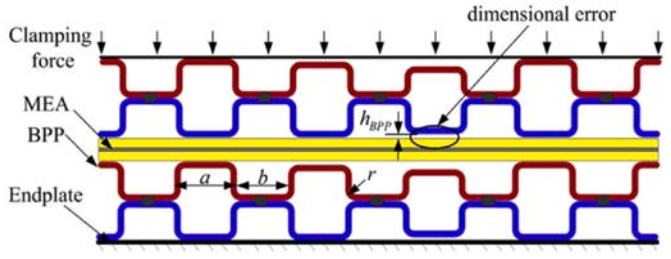

Fig. 4. Dimensional error of BPP [28].

During the assembly process, it is difficult to obtain the parameters of the fuel cell stack directly, which poses a significant challenge for assembly techniques. In terms of scientific literature, most of the research on PEMFC assembly techniques concerns the mechanical simulation model of the stack [30,35,36] and stack mechanical and performance tests [28,37]. There are also some studies involving stresses on components and stack assembly loads [31,33,38], as well as review studies [24,39,40]. Few of the current articles summarise the contents of the assembly techniques. The study presented in Ref. [39] carried out a detailed review of catalyst deposition and BPP manufacturing techniques, but left the assembly techniques for further study. In contrast, the review carried out in Ref. [24] analysed the effects of various forms of stress on fuel cells. However, research methods for determining the best assembly were not summarised. Similarly [40], reviewed the effects of mechanical compression on fuel cell components, but did not address the optimisation of the assembly load. The present work reviews various subjects related to fuel cell assembly, aiming to supplement and improve upon the conclusions in the existing literature. The development trend of the assembly technique is analysed to provide a reference for scholars engaged in relevant research. In order to highlight the most important characteristics of each technique, the conclusions from the available literature are analysed and integrated. The difficulties and challenges of PEMFC stack assembly techniques mainly involve the following aspects:

(1) Determination and optimisation of assembly load.
(2) Effect of assembly load on fuel cell components and performance.
(3) Research methods and means of assembly process.
(4) Combination of fuel cell design and automatic assembly.

The remainder of this paper is organised as follows: Section 2 focuses on the effect of assembly load and distribution on fuel cell components and performance. The effects of assembly load on fuel cell components such as the PEM, GDL, and CL are reviewed. Through the compression effect, the characteristics of the fuel cell such as electronic conduction, contact resistance (CR), and heat transfer are also affected. The optimisation of the assembly load and the realisation of uniform load distribution are reviewed in Section 3. Section 4 focuses on research on the fuel cell assembly mechanism, namely different assembly forms. Section 5 introduces related research on automatic assembly and points out the importance of automatic assembly for fuel cell industrialisation. Finally, after understanding the research content and progress of the stack assembly technique at this stage, Section 6 summarises the assembly technique and proposes future research directions. This review of the assembly technique can be used as a reference by PEMFC stack assembly researchers and engineers. The relevant conclusions and research contents offer significant guidance in the processes of PEMFC stack design and assembly.

2. Assembly load

A PEMFC stack achieves effective sealing and close contact between single cells through various assembly load holding devices. The assembly load and its distribution are two key factors affecting the output characteristics of the PEMFC stack. The stack maintains its compression

state through the assembly load. Under the assembly load, the components inside the stack produce stress owing to the assembly load [41]. The assembly load can be achieved by a point load, line load, or surface load [42]. Among them, the point load design has been studied most widely [34,43,44]. In this design, the bolt arrangement and assembly load are considered to be the most important factors affecting the uniformity of the pressure distribution in the fuel cell assembly [45,46]. Usually, The bolts arranged at the edge of the EP are easy to make the sealing ring around the flow field bear more load [47] (Fig. 5). The assembly load causes uneven compression of the GDL, thereby altering its porosity and gas permeability [48]. Studies show that the output characteristics of a PEMFC stack are closely related to the assembly load [49]. Therefore, the assembly force mainly affects the CR between the GDL and the BPP. A reasonable contact pressure distribution can improve the thermal conductivity by affecting the CR, and thereby improve the power of the fuel cell. It has been reported that the CR is a function of the assembly force, and most of the total power loss of fuel cells is caused by the CR between the BPP and the GDL [50]. The structure of the BPP and the force applied during assembly greatly influence the performance and lifetime of PEMFCs. Owing to the limitations of the manufacturing process, the height of the flow channel of the BPP cannot be ensured to be uniform. Therefore, when the BPP contacts the GDL, an uneven compression load is generated owing to the height difference of the land (rib). Owing to the extrusion of land, GDL area under land bears more assembly load than the GDL area under the channel [51]. The uneven stress of the GDL significantly influences the porosity, conductivity, and ICR, thus causing an accumulation of liquid water [52] (Fig. 6). The uneven distribution of contact pressure on the MEA results in an uneven distribution of current density and heating, which may cause hot spots in the MEA, as shown in Fig. 7. Therefore, the design of the assembly force is the first problem to be solved in the assembly technique. The assembly force should be maintained within a reasonable range [53]. If the assembly force exceeds a certain upper limit, the mechanical stress increases, which may also lead to the damage of the GDL, PEM, and cracking of brittle parts [54]. Similarly, an assembly force below the lower limit causes a series of problems such as leakage [55]. Fig. 8 summarises the factors that affect the assembly load and the reflection of the assembly load on the stack components. Table 1 summarises the problems caused by an unreasonable assembly load. This section summarises the research on assembly load from three aspects: the influence of assembly on fuel cell components and performance, and the distribution of assembly load.

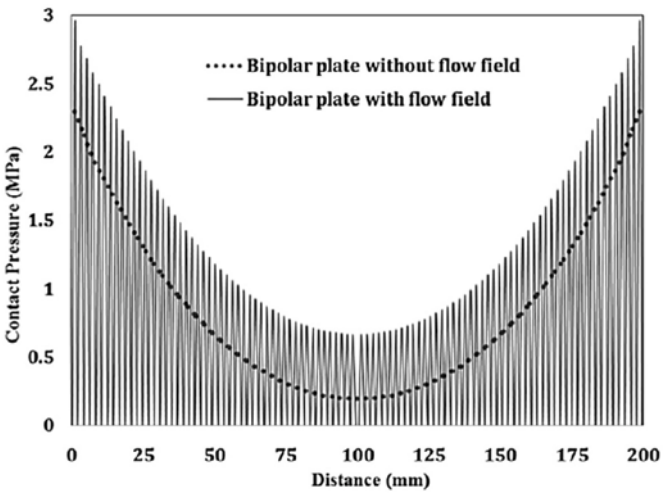

Fig. 5. Pressure distribution of point load [47].

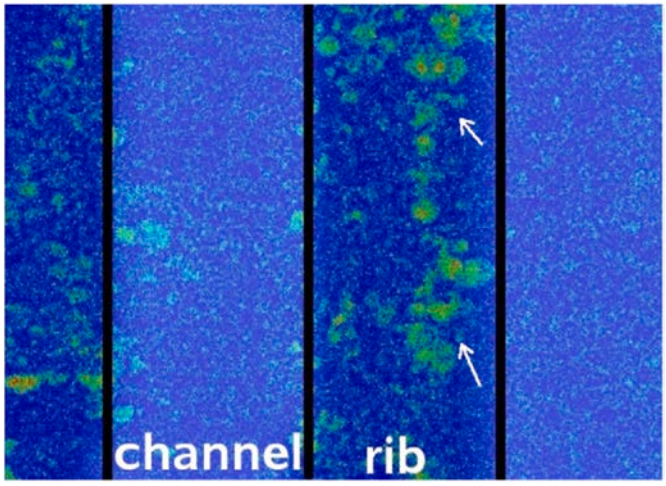

Fig. 6. Accumulation of liquid water (bright spots) [52].

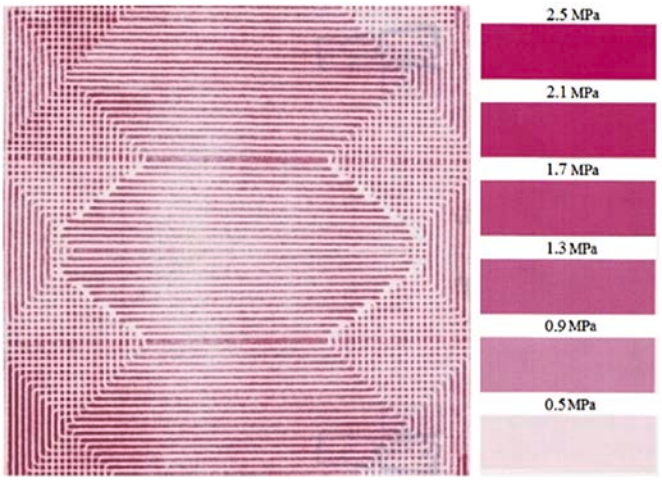

Fig. 7. Pressure distribution of membrane electrode assembly (15-cell stack) [47].

2.1. Effect of assembly load on PEMFC stack components

Assembly load has a significant impact on the performance and durability of the PEMFC stack. The main components of PEMFCs are PEMs, CLs, GDLs, BPPs, gaskets, and EPs. First, the influence of assembly load on the main PEMFC components is reviewed.

2.1.1. Assembly effect on PEM

The PEM is a key component of PEMFCs, which can separate hydrogen gas and oxidant gas, and transport hydrogen ions and water at the same time. The PEM only allows the protons generated by the anode to pass through, while blocking the electrons generated by the anode from passing through the membrane, thereby forcing the electrons to pass through the external circuit to reach the cathode. The PEM must have excellent chemical properties, mechanical ductility, water absorption, and proton conductivity [59]. In general, the material forming a PEM is a type of polymer. The properties of the membrane determine the main technical characteristics of the fuel cell structure and operation. Solasi et al. [67] studied the hydration and dehydration processes of a PEM under the assembly force through numerical simulations. They found that water absorption or dehydration of the membrane would make the PEM further expand or contract under the original assembly load. They discussed PEM failure modes by establishing a durability model of the PEM. The hydration and dehydration cycles produce

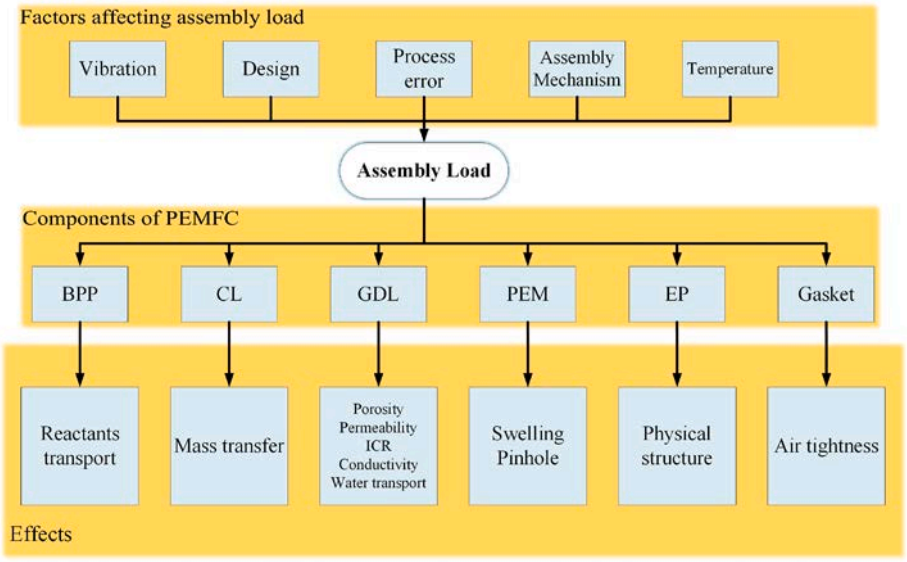

Fig. 8. Effects of assembly load on PEMFC stack components.

Table 1
Effect of assembly load on PEMFC stack components.

Component	Effects (high assembly load)	Effects (low assembly load)	Reference
PEM	• Developing mechanical strain; • Contribute to hydration/ dehydration strain; • Buckling or delamination of PEM; • Pinhole/cracks.	• Improve the porosity and wettability; • Reduce some of the high stress spots onto the rest of the MEA during stack compression.	[54, 56–67]
CL	• Decrease the mass transfer rate.	• Increase the water and reactant gases transfer.	[36, 68–79]
GDL	• Decrease in porosity and permeability; • Reduce the ICR of GDL; • Improve the bulk conductivity; • Higher mass over-potential; •Lower electrical and thermal resistance in GDL.	• Increase in porosity and permeability; • Improve the gas transfer; • Higher ICR; • Reduce the bulk conductivity;	[80–100]
BPP	• Block gas diffusion; • Blockage of liquid water.	• Higher ICR between GDL and BPP; • Gas leakage; • Faster gas flow.	[90, 101–116]
Gasket	• Material degradation; • Thickness reduction.	• Gas leakage.	[55, 117–122]
EP	• Poor load distribution; • Larger deflection.	• Better load distribution; • Smaller deflection.	[42, 123–128]

significant stress in the membrane when the fuel cell bears the assembly load. In extreme cases, it causes pinholes in the membrane, which lead to material degradation. Therefore, the study of mechanical stress on the PEM can help to gain a deeper understanding of the action and mechanism of assembly load.

De et al. [57] studied the pressure distribution of a 3 kW fuel cell stack with a nominal bolt torque of 20 psi. The pressure distribution on the membrane was obtained by numerical simulation, and the safety stress threshold of the membrane under the nominal torque was obtained. When the stress is within the safe threshold, even if the moisture content of the membrane is in the extreme state, it will not cause irrecoverable deformation on the membrane. A pressure film was placed on both sides of the PEM to verify the simulation results. The results show that the stress of the membrane is mainly concentrated on the edge (as shown in Fig. 9). When the assembly force increased, the stress on the membrane increased along the axial direction, and the stress concentration generally does not appear in the central area. The conclusion emphasises the importance of using a semi-rigid gasket to protect the MEA in a practical assembly. In the design of fuel cell components, special consideration shall be given to the gas inlet and outlet areas and the contact area between the MEA and BPP to avoid stress concentration. Bograchev et al. [58] established a linear elastic–plastic two-dimensional model considering the main components of a fuel cell. The actual loading process of the bolt was simulated, and the stress distribution on the MEA was analysed. The developed model can help to better understand the local and global stress distribution of the MEA in the assembly process. Locally, the stress distribution is uneven under an

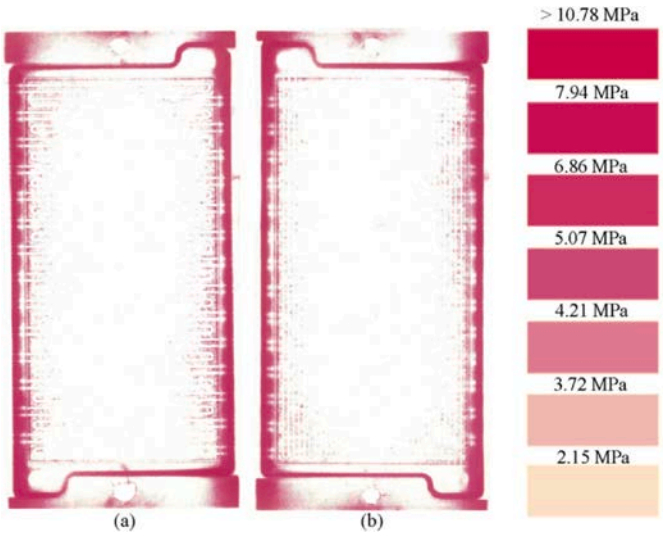

Fig. 9. Experimental results of pressure film: (a) cathode side, (b) anode side [57].

independent channel. From the global perspective, this type of inhomogeneity is periodic. Similarly, their research also confirmed that there is a large non-uniform stress on the contact surface between the membrane and the sealing joint. The non-uniform stress is mainly caused by the difference in stiffness between the membrane and the gasket, and it is related to the structure of the gasket. The results showed that when the applied assembly load was more than 1 MPa, the plastic deformation of the membrane began.

In fact, the influence of mechanical stress produced by assembly on a PEM is complex, which is a comprehensive effect of multiple stresses superimposed on each other. In the actual operation of a fuel cell, the membrane stress changes owing to the expansion of water absorption and temperature fluctuation [62]. In the process of membrane expansion, owing to the uneven distribution of assembly load, membrane cracking or pinhole formation may occur at points of locally high stress. This causes cross-leakage of the reaction gas, thus reducing the output power of the stack and ultimately leading to a failure of the hole stack [64]. Because the water absorption and temperature change of the fuel cell are dynamic, the highest stress on the membrane is also changing. Although a high assembly load may lead to buckling of the whole MEA, it is generally considered that the CL and GDL have sufficient strength to ensure the flatness of the membrane. It is very difficult to measure the local stress on the membrane due to membrane buckling caused by changes in the temperature and water content of the membrane [65]. This is the superposition of the internal chemical effect and mechanical effect caused by assembly that leads to failure of the membrane [66].

Therefore, it is difficult to quantify the influence of assembly load on PEM alone. There are two reasons: first, the change of water content and temperature of PEM will produce mechanical stress on PEM, which will offset the assembly load to a certain extent. Second, when the fuel cell is working, the mechanical stress generated on the PEM is in the process of dynamic fluctuation, which is difficult to measure.

2.1.2. Assembly effect on CL

The CL is where the electrochemical reaction occurs. At present, platinum (with ionomers) is widely used as a catalyst for the electrochemical reaction of hydrogen and oxygen in PEMFCs, and carbon is used as a catalyst carrier [75]. To improve the efficiency of the reaction and the performance of the PEMFC stack, it is necessary to maximise the contact between the reaction gas and the CL. At the same time, the CL also needs good mechanical properties to avoid crushing due to the excessive assembly load [76]. In general, there is an MPL composed of carbon and hydrophobic adhesive on the contact side of the GDL and CL, whereas the GDL is generally a carbon fibre paper or carbon cloth with a network structure [77]. Under the joint action of the GDL and MPL, the contact side of the GDL and CL easily produces a high stress point caused by the assembly force [78]. When the stack bears an excessive assembly load, it a large stress is produced on the CL and MPL.

Malekian et al. [78] investigated the effect of compression on the deformation of the CL. Two key values (2 MPa and 5 MPa) of CL load were obtained by compression tests on five different CL samples. The results show that when the load on the CL is less than 2 MPa, elastic deformation of the CL occurs. Even after 12 cycles of loading, the deformation of the CL remains linear without plastic deformation. However, when the load is more than 5 MPa, plastic deformation and work hardening begin to appear in the CL. Under cyclic compression, the plastic deformation was more obvious, indicating that the microstructure of the CL changed. In their next study, using the effective medium theory, a CL compression analysis model was established to simulate the impact of compression on CL characteristics [69].

The pore size distribution (PSD) and porosity of the CL are the two main indices to describe the microstructure of the CL [70]. Malekian et al. [71] analysed the change in pore size distribution and porosity of the CL under compression to explain the microscale effect of the assembly load on the CL. They used the geometric model in their previous work [69] to simulate the random distribution of the CL pore size. The effects of compression on four different CLs were studied, and the simulation results were compared with previous experimental data. The results show that the change in pore size is a function of compression and is related to the initial porosity, PSD, and material properties of the CL. The pore size of the four types of CL decreased by 20%–50% when the CL was loaded with 5 MPa. This change should be considered when studying the mass transfer characteristics of the CL under an assembly load. The results also show that when a CL is compressed, the number of large pores decreases and the number of small pores increases.

More work in the future may focus on the specific components of CL. That is, whether CL with different formulations still has good mechanical stability under assembly load, especially in long-term test.

2.1.3. Assembly effect on GDL

The GDL is made of conductive porous materials with high porosity. The substrate is usually graphitized carbon paper or carbon cloth, and the surface is coated with polytetrafluoroethylene (PTFE), which exhibits hydrophobicity. The GDL requires a certain mechanical strength to support the CL and prevent crushing due to the assembly load. At the same time, it has a larger porosity and hydrophobicity, such that the reaction gas and water can pass through the diffusion layer in time [96]. The characteristic parameters of the GDL, such as porosity and permeability, affect the rate of the electrochemical reaction, and thus influence the output characteristics of the PEMFC stack [97].

Owing to the soft and brittle structure of the graphite fibre, the GDL can easily be deformed or damaged by the BPP when the stack receives the assembly load. The GDL has two compression states under an assembly load. As shown in Fig. 10: (1) under the land (rib), when the GDL is loaded, the GDL fibre is squeezed and deformed; therefore, the porosity under the land decreases, which slows down the diffusion of gas to the CL, and causes the accumulation of liquid water; (2) under the channel, the GDL is essentially not compressed, and the flow of reaction gas and water is principally unaffected. However, the GDL on both sides is squeezed by the BPP, which leads to the GDL fibre invading the flow channel. Therefore, the geometry of the BPP must be considered when studying the effect of the assembly load on the GDL. When the assembly load is excessive, the contact surface of the land and channel produces a large shear force on the GDL, which causes damage [98]. Because of the complex fibre structure, it is difficult to study the effect of compression on the GDL. The different lengths, thicknesses, and directions of the fibres cause different degrees of deformation under compression. It is possible that plastic deformation occurs in some regions when elastic deformation occurs in most areas of the GDL. The generation of mechanical failure is related to the direction of the fibre, the force of nearby fibres, and the structure of the BPP [99].

Gaiselmann et al. [88] further confirmed the two types of GDL deformation mentioned above by generating three-dimensional (3D) analogue images of a GDL under various degrees of compression. They introduced a parametric model to describe the microstructure of fibre materials in a GDL under compression. The model can generate images of the GDL under different compression ratios (as shown in Fig. 11), which helps to better understand the uneven pressure distribution of the GDL under BPP compression. The model is verified by comparing the microstructure characteristics of simulated compression with those of real compression. As the BPP is composed of a series of lands and flow channels, this structure produces an uneven assembly load distribution on the GDL, which is a notable feature of PEMFC assembly. This type of uneven load distribution affects the mass transfer characteristics under lands and flow channels, and the mass transfer may be different between them by up to a factor of two [89].

The uneven assembly load distribution on the GDL also affects the temperature distribution. Owing to the non-uniform compression of the GDL, the thermal contact resistance of the interface between the GDL and BPP is different. The contact resistance under the channel increases the heat loss, such that the reaction rate under the channel changes significantly. The contact resistance of the contact interface under the

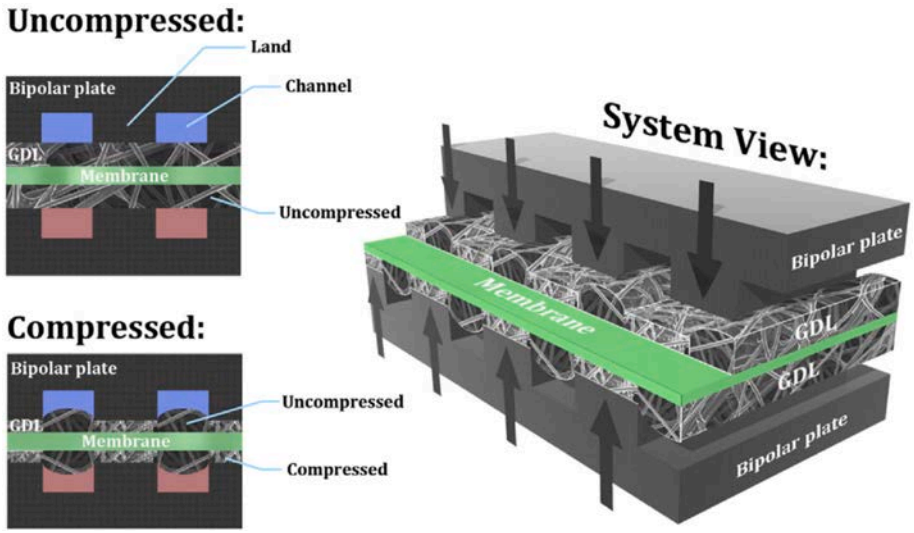

Fig. 10. Two forms of GDL deformation [48].

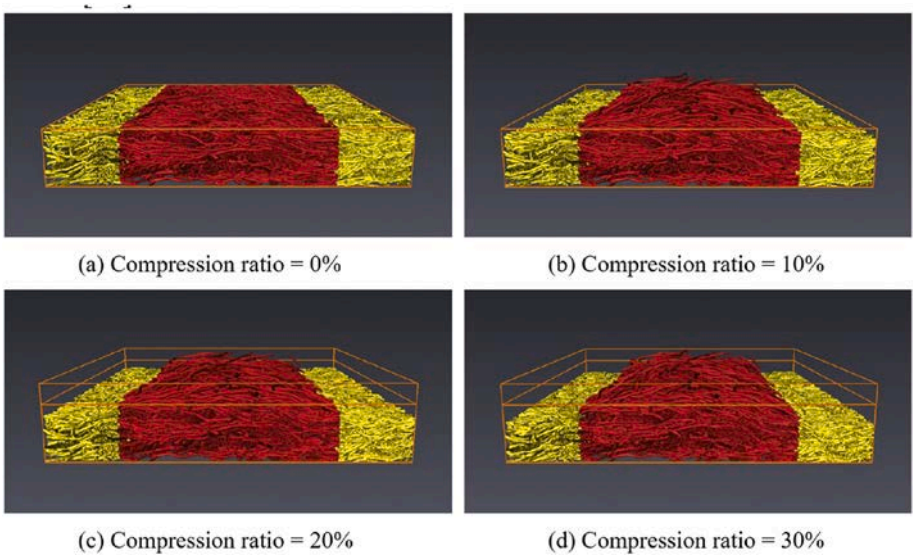

Fig. 11. Three-dimensional simulation image of GDL with different compression ratio. The yellow (red) marked fibres are located underneath the land (channel) [88]. (For interpretation of the references to colour in this figure legend, the reader is referred to the Web version of this article.)

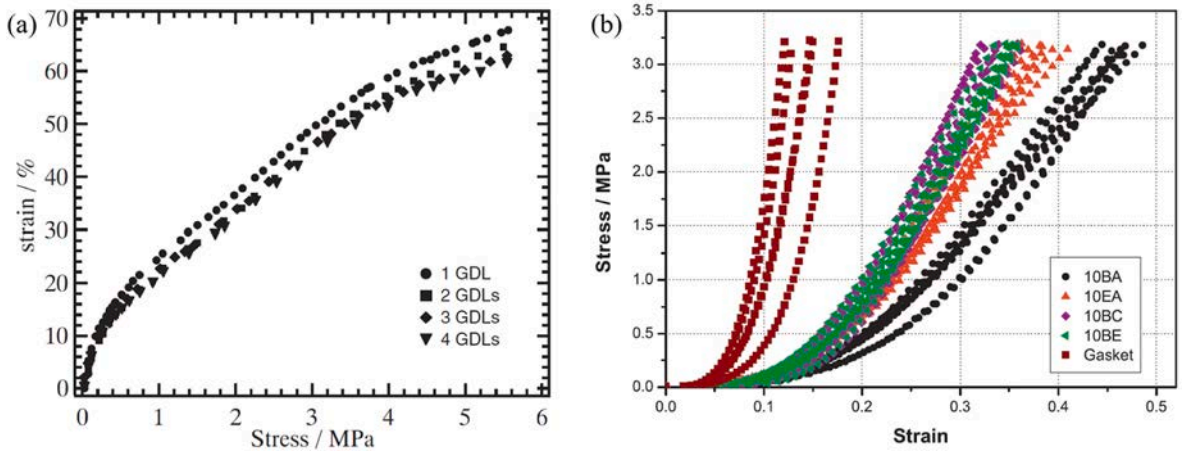

Fig. 12. GDL stress–strain curves [83,84].

land is low, such that the heat generation is low and the temperature is low. The heat generated in the electrode under the channel flows laterally and enters the GDL region under the land, which results in a significant temperature gradient in the cell [100]. This temperature gradient is significant for the design of fuel cells. The high-temperature area affects the performance of the material, causes material decay, and reduces the lifetime. Therefore, the temperature distribution should be as uniform as possible to improve the performance of the entire stack [82].

Nitta et al. [83] studied the relationship between stress and strain of the GDL. When the stress increases from 0 to 5.5 MPa, the stress–strain curve of the GDL presents a nonlinear region and two linear regions, as shown in Fig. 12 (a). It can be concluded that the mechanical property of the GDL is a function of the assembly load. Further stress–strain curve analysis was carried out by Ismail et al. [84]. The stress–strain curve in Fig. 12 (b) is similar to that in Ref. [83], that is, the stress–strain curve of the GDL is composed of two linear regions and one nonlinear region. When the stress increases from 0 to 0.01 MPa, the strain increases linearly with the increase in stress. Owing to the fluffy structure of the GDL, in the initial stage of applying an assembly load, the GDL has elastic deformation, which plays a buffering role. When the stress is further increased to approximately 1 MPa, the strain increases nonlinearly with the increase in stress, and the gradient is small. This indicates that plastic deformation of the GDL material begins, which can be explained by the increase in the contact area between the GDL material and BPP, and the decrease in the pore size of the GDL [85]. With a further increase in stress, the stress–strain curve enters the second linear region. Relevant research also showed that the stiffness of the GDL increased with the increase in PTFE content. This is because the porosity of the carbon carrier is reduced, and PTFE is more closely bonded. In addition, the MPL on the contact side of the GDL and CL can also significantly improve the stiffness of the GDL [108]. In fact, there will be a ring of gaskets around the GDL. Therefore, when the assembly load is applied to the GDL, the stiffness and deformation of the gasket should be considered in the deformation of the GDL. In the actual assembly process, the strain on the GDL is controlled by the initial thickness and compressibility of the gasket [87].

After a certain degree of compression, the porosity of GDL material decreases. On the other hand, compression makes the fiber connection of GDL more compact, which is the reason for the reduction of contact resistance. However, extreme compression of GDL will lead to fiber fracture and GDL crack [104,129–132]. As shown in Fig. 13. Fig. 13 (a) shows the intact GDL surface under the digital camera. Fig. 13 (b) shows the cracked GDL surface under the digital camera. Fig. 13 (c) shows the scanning electron microscope (SEM) image of GDL after over compression. The crack of GDL fiber can be clearly seen from the SEM image. Kim et al. [133] studied the effect of cracked GDL on the performance of fuel cell, and pointed out that the cracked GDL had an effect on the concentration loss of PEMFC performance. It is pointed out that the narrower the flow channel, the greater the performance loss. This was further confirmed in the study of Chen et al. [25]. Chen et al. [25] pointed out that the over compression of GDL greatly increased the mass transfer resistance. After gradually applying 2Nm, 4Nm and 7Nm torque to the fuel cell stack, a clearer microscopic image of GDL crack was observed. As shown in Fig. 14. The effect of GDL crack on concentration loss is more obvious in the polarization curve, which will be discussed later.

Porosity is an important parameter of GDL. The porosity of the GDL affects the transport process of gas and water, which is closely related to the output characteristics of the fuel cells. When subjected to an assembly load, the GDL and BPP are compressed, and the intrusion phenomenon mentioned above occurs. Not only does the contact resistance change, but so do the porosity and permeability [134,135]. The GDL should have appropriate porosity and permeability to guide the reaction gas to the CL, as well as to effectively transport the water generated at the CL. When the GDL is compressed, the conductivity increases and the porosity decreases, which hinders the transport of the reaction gas in the GDL. The blocking effect is more obvious when the cathode gas is air [136]. The gradual distribution of PTFE in the GDL is usually used to improve the interaction between conductivity and porosity [137]. This type of GDL with a porosity gradient can reduce the water content near the BPP side, avoid flooding, and maintain a certain humidity on the CL side [138,139].

Chien et al. [140] pointed out that the compression ratio of the GDL and the rate of channel intrusion increased linearly with an increase in the assembly load. The results show that the average porosity decreases linearly, and the contact resistance decreases nonlinearly. The combined effect of porosity and contact resistance should be fully considered in designing the optimum assembly load. Chi et al. [81] proposed a non-uniform compression model that more closely approximates a real assembly. The results show that a larger compression ratio results in a smaller the pore size of the GDL. A smaller pore size can increase the cross-sectional area of charge transfer and reduce the high-frequency resistance and ohmic polarization, but a small pore size is not conducive to the discharge of liquid water. Under a high compression ratio, the current density distribution is uneven, and the current density in the downstream decreases significantly, owing to flooding caused by high saturation. Fuel cells sometimes start up at temperatures below 0 °C. Existing studies have shown that high porosity is not conducive to the complete discharge of water through purging [137]. The freezing of water causes the membrane structure to be destroyed. Therefore, the porosity of the GDL should be reasonable. Generally, a porosity of approximately 0.6 is conducive to improved performance [137]. In addition, for inhomogeneous compression, the porosity distribution under the channel is slightly different from that of the GDL prior to compression [141]. It is worth noting that temperature and humidity changes during fuel cell operation may lead to the uneven deformation of the GDL and the expansion of the membrane [56,92]. The

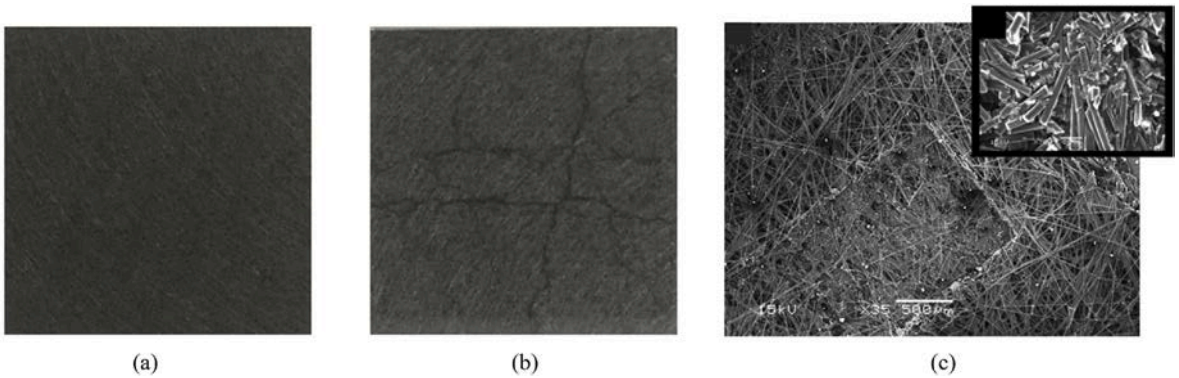

Fig. 13. (a) Intact GDL surface under the digital camera (b) cracked GDL surface under the digital camera [133] (c) SEM image of GDL after over compression [129].

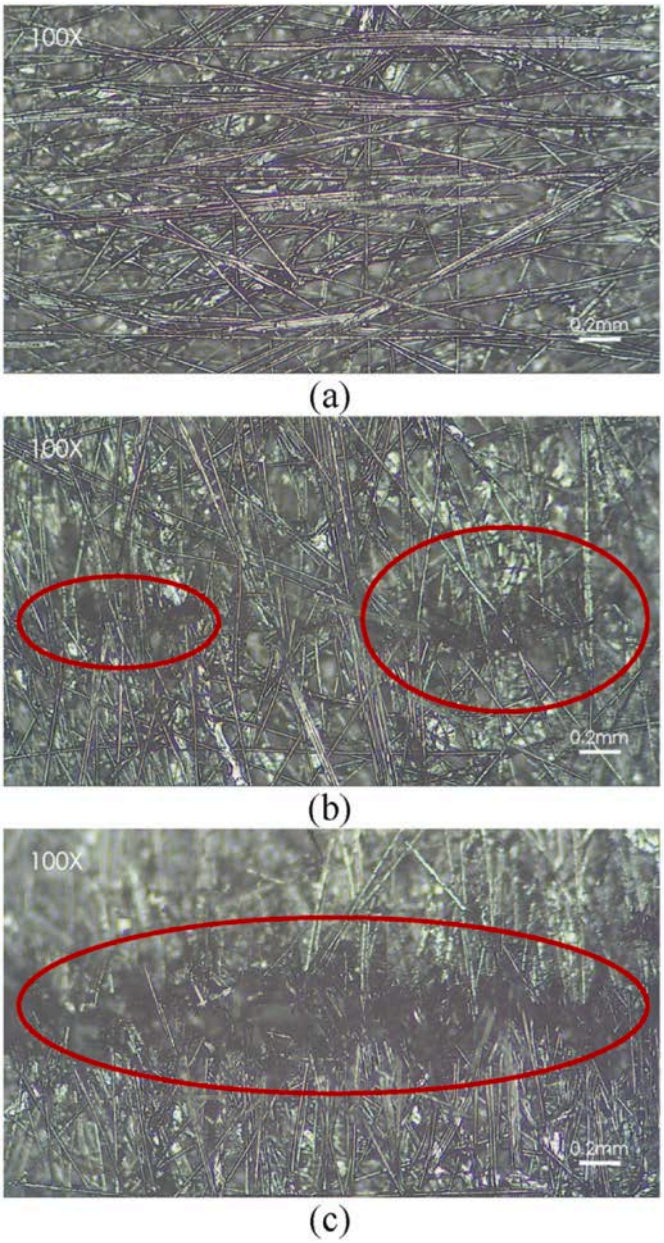

Fig. 14. Microscope image of GDL after compression: (a) 2Nm, (b) 4Nm and (c) 7Nm [25].

redistribution of contact pressure also affects changes in porosity, which should be fully considered when the assembly load is applied.

Under the assembly load, GDL intrusion occurs, the thickness of GDL decreases and the porosity decreases. It is worth noting that under the action of assembly load, the effects of GDL intrusion, GDL porosity and GDL thickness are interrelated. Therefore, it is important to pay attention to the simultaneous impact of the three factors. Toghyani et al. [142] systematically studied the simultaneous effects of GDL intrusion, GDL porosity and GDL thickness on the overall performance of fuel cells by using finite element analysis and computational fluid dynamics. The authors pointed out that the assembly load will reduce the porosity and thickness of GDL. Under assembly load, GDL intrusion will reduce the performance of fuel cell. However, the decrease of GDL thickness and GDL porosity has little effect on the performance of fuel cell. The porosity of GDL decreases, the gas transmission is blocked, and the performance of fuel cell decreases.

GDL has always been the research focus in the assembly process. Under the assembly load, on the one hand, the contact resistance is improved, on the other hand, the porosity is reduced. The best fuel cell performance requires a compromise between these two effects. In recent years, the research on GDL under assembly load has also focused on this problem. However, the compressibility of GDL is largely limited to gaskets. At the same time, in the actual working process of fuel cell, icing will cause irreversible damage to the fibre structure of GDL. Therefore, future research needs to pay more attention to the relationship between GDL and gasket under assembly load. In order to obtain a good GDL assembly state, the thickness and material of the gasket must be comprehensively designed. At the same time, how to reduce the influence of icing on GDL and keep it in the best compression state is worthy of in-depth study.

2.1.4. Assembly effect on BPP

The BPP collects the current generated by the electrochemical reaction, isolates hydrogen and air, and transports hydrogen to the anode and air to the cathode. Each BPP in the stack is related to two single cells. One side of the BPP is the anode plate of a single cell, and the other side is the cathode plate of the adjacent cell. The middle cavity of the two plates is the coolant channel. Both sides of the BPP are processed into the flow channel of the reaction gas. There are many structural forms of the flow channel, and the process of transferring the assembly load depends on the structural form.

The strength of the BPP is remarkably high, and the assembly load does not cause mechanical damage in general. The influence of the assembly load on the BPP mainly concerns the gas flow in the flow channel and the ICR between the BPP and GDL [111]. The intrusion of the GDL into the flow channel under an assembly load reduces the effective cross-sectional area of the flow channel, which affects the gas flow. Regardless of the particular structure of the flow channel, the assembly load increases the depth of the GDL into the flow channel, thereby increasing the gas flow rate [90]. Fig. 15 depicts the velocity vector plot at the centre line of the channel under different assembly loads (GDL intrusion depth). It can be seen that the initial gas velocity has a linear relationship with the assembly load. In the subsequent flow process, the gas velocity shows parabolic acceleration. Research on BPP compression proved that the ICR between the BPP and GDL is determined by the size and distribution of the assembly load, and the minimum contact resistance can be obtained by a constant and uniform pressure distribution. The ICR varies nonlinearly with the assembly load [112,113], as shown in Fig. 16. In the initial stage of compression, the ICR decreases rapidly with the assembly load. Then, with further increases in the assembly load, the ICR changes more slowly. This is because in the initial stage of compression, the assembly load is small, and the contact between the BPP and GDL is characterised by point contact between rough surfaces. Therefore, the ICR is very high and decreases rapidly with the increase in assembly force [109,112,114]. Zhou et al. [109] analysed the effect of the assembly load on the ICR between the BPP and GDL. A finite element model (FEM) of the ICR was established to analyse the contact resistance under different land widths and assembly loads. The results showed that for graphite BPPs, increasing the assembly force and land width can reduce the ICR. For stainless steel BPPs, there is an optimum land width to obtain a lower ICR and higher porosity.

Manufacturing errors and the geometric structure of the BPP channel also have some influence on the assembly. Based on the current manufacturing techniques and assembly level, there are three main types of BPP errors: (1) dimensional error of channel height change, which is mainly related to manufacturing technique; (2) shape error, which is related to the residual stress in the stamping process and thermal stress in the welding process [98,102,115,116]; and (3) assembly error, which is determined by the assembly process and related to the assembly mechanism. These common errors will further increase both the difficulty and cost of assembly. Three common errors are shown in Fig. 17. Peng et al. [103] studied the influence of these three types of errors on the fuel cell stack performance. The geometry of the BPP

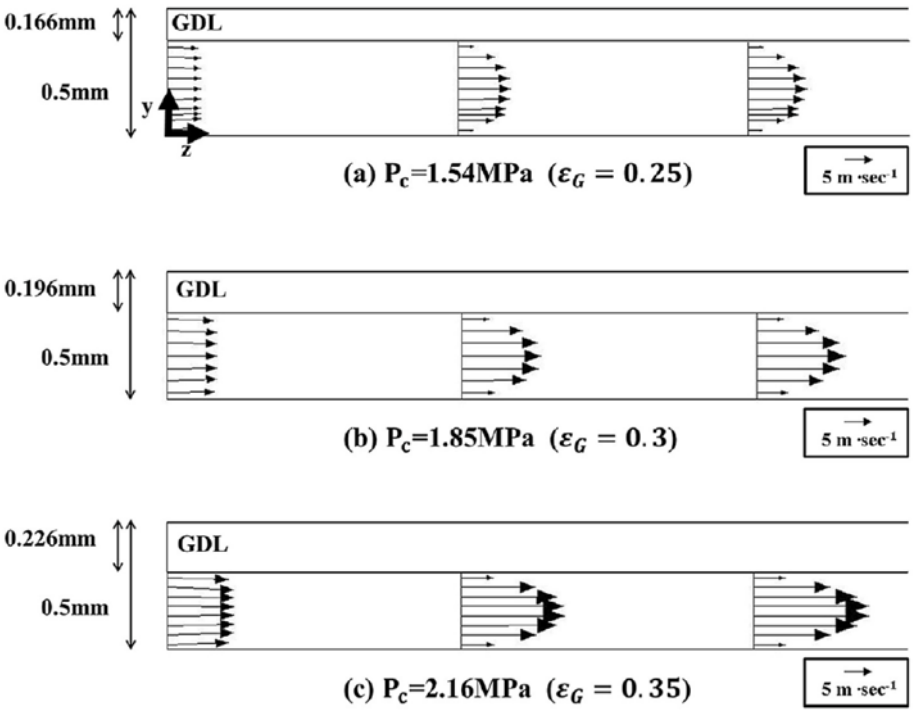

Fig. 15. Gas flow in the flow channel [90].

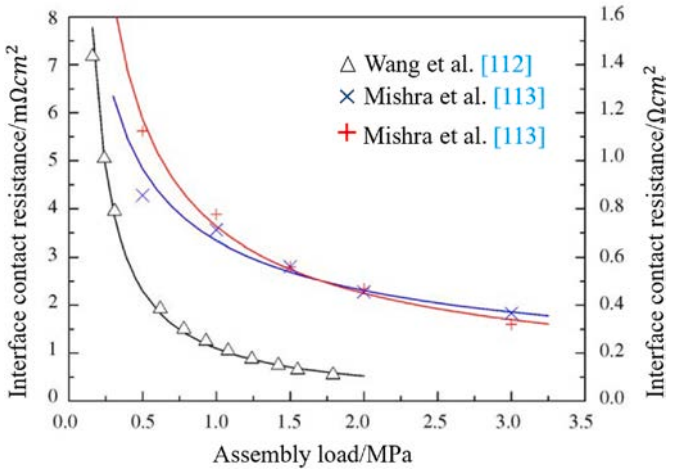

Fig. 16. Interface contact resistance and assembly load curve.

channel also affects the distribution of the assembly load to a certain extent. The geometry of the channel is usually trapezoidal or rectangular, which causes stress concentration at the inflexion point of the fillet. Under the assembly load, the contact stress at the fillet is more than twice that at the channel [104], and the stress increases significantly with the decrease in the fillet radius [104,105]. This causes more physical damage to the MEA in contact with the fillet, thus affecting its chemical properties. Nitta et al. [106] proved that the local stress causes local changes in mass transfer and charge transfer, and has a significant effect on the current density distribution. This phenomenon is explained theoretically using a model [107]. The local stress at the fillet may damage the physical structure of the CL, as shown in Fig. 18.

In addition, the influence of assembly load on the performance of fuel cell is related to the geometry of flow channel. The three common channel types are serpentine, parallel and interdigital channels. As shown in Fig. 19. According to different working conditions and channel types, the optimal assembly load of fuel cell stack is analysed. Li et al. [143] established a three-dimensional and two-phase flow mathematical model to study the effect of GDL intrusion on the performance of fuel cells with interdigital flow channel. It is pointed out that for interdigital flow channel, the performance of fuel cell has been greatly improved with the increase of assembly load. But at the same time, the gas pressure drop in the channel also increases significantly. On the premise of ensuring the air tightness, the authors suggest that the assembly load of fuel cells with interdigital flow channel should be as small as possible to reduce parasitic loss. Li et al. [144] used the finite element method to study the effect of the invasion of GDL on the performance of the fuel cell with serpentine flow channel. The results show that for the fuel cell with serpentine flow channel, the performance of the fuel cell first increases and then decreases with the increase of assembly load from 0 MPa to 5.0 MPa. The authors suggest that for fuel cells with serpentine flow channel, the assembly load should be kept in the appropriate range of 0.5 MPa–1.5 MPa in order to improve the output power of fuel cells. Son et al. [145] pointed out that at low current density, the performance of PEMFC with serpentine and parallel channels is mainly affected by contact resistance. At high current density, PEMFC with serpentine and parallel channels have the best performance at assembly load of 0.25 MPa and 0.5 MPa. For interdigital channels, higher assembly load and lower contact resistance are the main factors determining the current density. When using interdigital channel, the pressure drop change caused by assembly load should be considered. Therefore, it can be concluded that the assembly load should be determined according to the working voltage of the fuel cell and the geometry type of flow channel.

The good contact between BPP and GDL can effectively reduce the contact resistance, which is related to the type of BPP, coating and channel geometry. However, in fact, how to reduce the manufacturing error of BPP and improve the machining accuracy seems to be worthier of in-depth study.

2.1.5. Assembly effect on gasket

In order to achieve good sealing between adjacent BPPs or between the BPP and the current collector, it is necessary to place sealing rings/gaskets between adjacent components. To avoid the leakage of the reaction gas, the sealing material must be compressed to a certain extent.

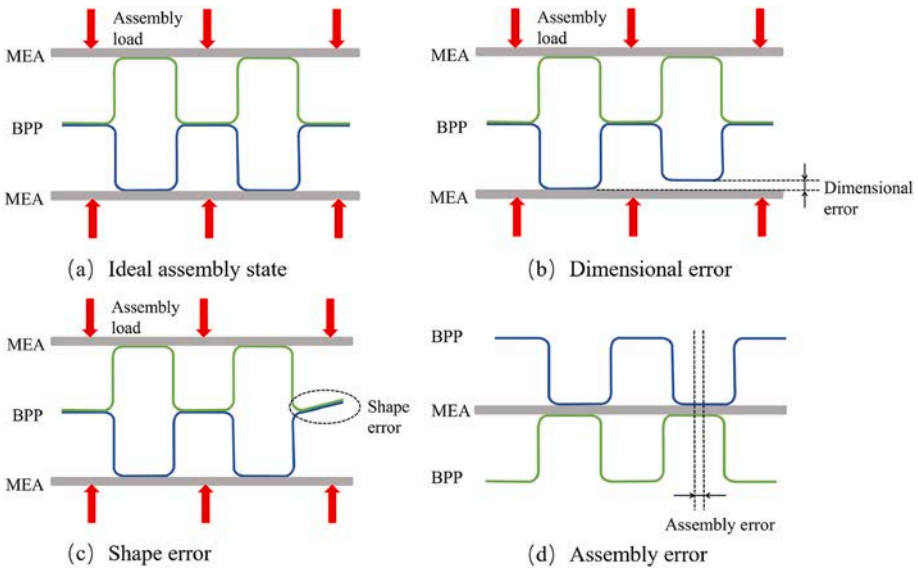

Fig. 17. Error types of BPP: (a) ideal assembly state, (b) dimensional error, (c) shape error, (d) assembly error.

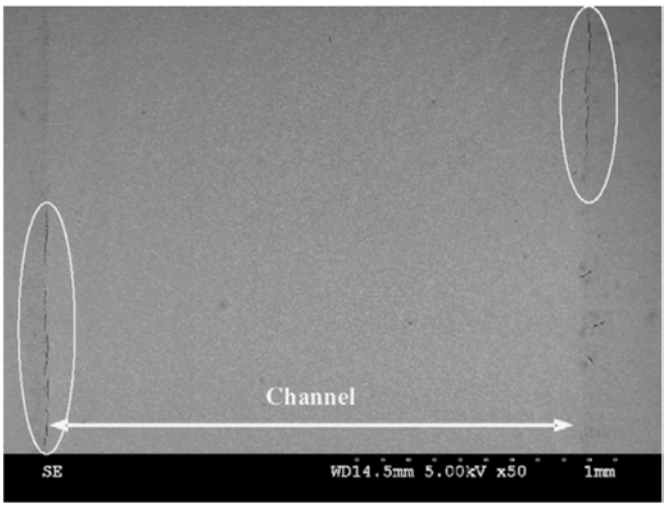

Fig. 18. Surface images of CCM under the channel [146].

The gasket is located in the sealing groove of the BPP, and its thickness is greater than the height of the BPP channel; therefore, it is the first component to be pressed in the assembly process. For the sealing performance of the stack, the design requirements of the assembly load are to ensure that there is no gas leakage inside the stack, and that the stress on the sealing gasket after the assembly load is applied is less than the yield limit of the material. Sealing determines the minimum assembly load [117]. As shown in Fig. 20, the sealing gasket is placed in the sealing groove of the BPP. The gasket contacts both the MEA and BPP. Under the action of gas pressure, the seal has the tendency to slide, and under the action of assembly load, the friction between the seal and the contact surface can prevent the sliding, so as to prevent the internal gas leakage of the fuel cell.

The durability of the fuel cell sealing ring is important to the sealing performance. Tan et al. [118] tested the aging mechanism of silicone rubber gaskets under an assembly load. A fixed assembly load was applied to the rubber sample, and its long-term degradation at 60 and 80 °C was observed by optical microscopy. The results showed that the higher the working temperature of the gasket, the faster its degradation. In addition, mechanical compression accelerated the degradation. Based on micro-images of gasket degradation, related works [119,120] also confirmed that the initial characteristic of aging is an increase in surface roughness. Over time, the surface of the sample hardens, Young's modulus of elasticity increases, and plastic deformation occurs [121]. Harsh working conditions eventually crack the silicone rubber. In a three-year durability test [122], it was observed that the thickness of the silicone rubber gasket decreased by approximately 25 μm, and the degradation of the gasket on the edge of the active zone was so significant that the silicone particles from the gasket were also observed on the surface of the gas diffusion layer. This leads to an increase in the GDL load and reactant transfer resistance. Therefore, the chemical

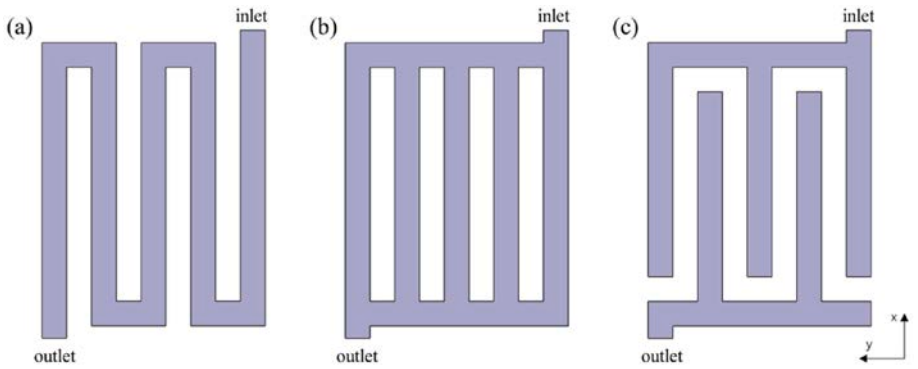

Fig. 19. Three geometry type of flow channel: (a) serpentine, (b) parallel, (c) interdigital.

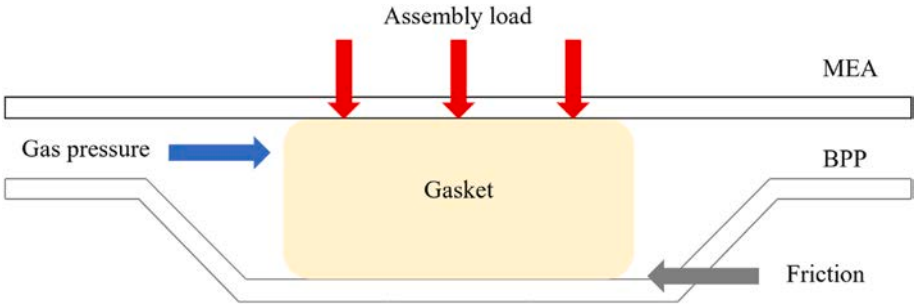

Fig. 20. Mechanical behaviour of gasket.

degradation and mechanical compression of silicone rubber affect the mechanical properties of the gasket. Gatto et al. [55] tested the effect of several common seal ring materials on the performance of fuel cells under an assembly load. The results show that different sealing ring materials cause different degrees of deformation of the GDL under the same assembly load, and then alter the characteristics of the fuel cell. This was also confirmed in Refs. [91,93]. For the test stack, the optimum assembly torque of a nitrite butadiene rubber (NBR) and expanded PTFE seal ring is 11 Nm, whereas the assembly torque of PTFE is 9 Nm. The calculation of the optimal assembly load includes the material properties of the seal ring, which should be considered in the design. In the future research, the influence of different methods for applying the gasket (injection molding, screen printing, dispensing or as separate piece) on assembly should be considered.

Through relevant literature research, it can be concluded that the influence of assembly load on the gasket is mainly reflected in three aspects: 1) the thickness of the gasket is thinner in the long-term test, which may have an adverse impact on the air tightness of fuel cell and lead to over compression of GDL; 2) The gasket is the key factor to control the assembly load applied to GDL. In order to obtain the ideal GDL compression state, it is necessary to comprehensively consider the initial thickness and material selection of the gasket; 3) Higher assembly load and working temperature will accelerate the aging of the gasket. The aging of the gasket starts from the increase of roughness until cracks appear. Substances released after aging of gasket can cause CL poisoning. Therefore, the selection of materials with high stability is an important factor to improve the durability of gaskets.

2.1.6. Assembly effect on EP

The EP of the fuel cell can operate in conjunction with a fastener to provide an appropriate assembly load for the stack and control the internal contact pressure distribution. Its mechanical characteristics have an important impact on the overall performance of the fuel cell stack. The required EP characteristics for good performance include sufficient strength and rigidity, small volume, light weight, and ease of processing.

The influence of the assembly load on the EP mainly relates to the deflection of the EP [42]. Deflection is the results caused by thickness and assembly load. Asghari et al. [123] established an FEM to study the influence of the EP thickness on the deflection of the EP and the assembly load distribution. Considering the cost of the EP design, the reference value of the optimal EP thickness is given. The finite element analysis showed that the four corners of the EP would be deformed

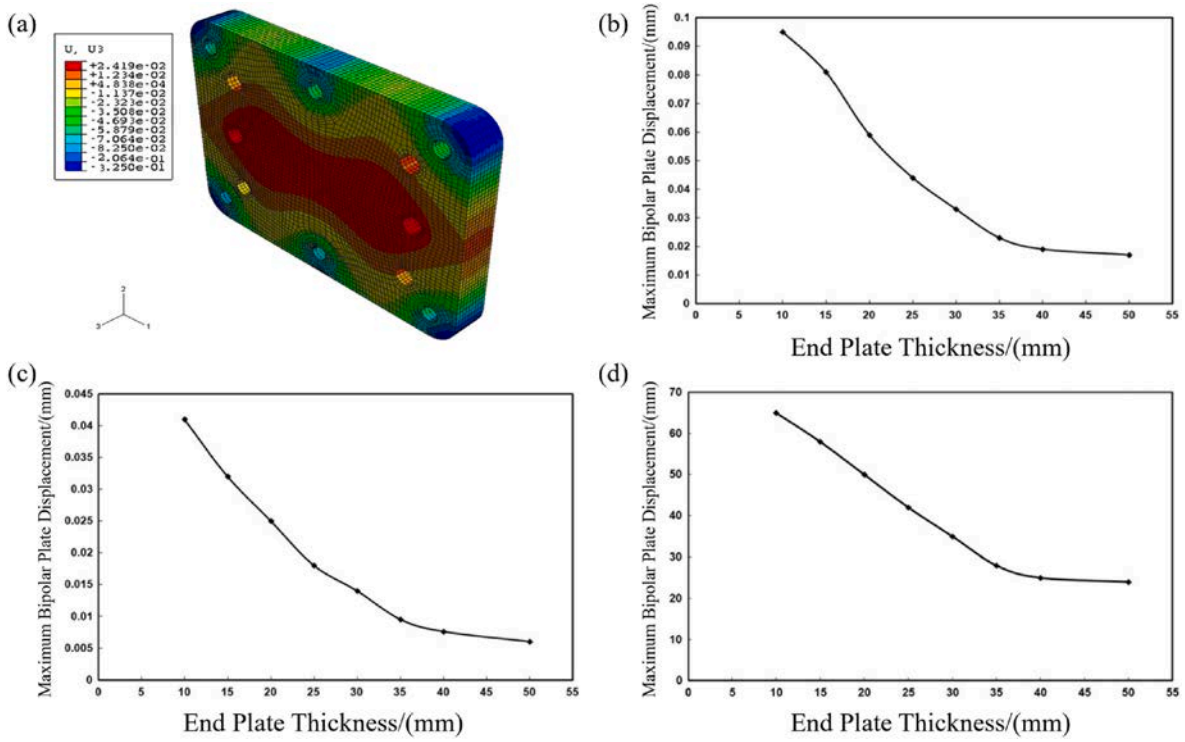

Fig. 21. (a) EP deformation; effect of EP thickness on (b) maximum EP displacement, (c) maximum. BPP displacement, and (d) maximum principal stress in BPP [123].

inward and the centre of the EP would move outward under an assembly load (as shown in Fig. 21 (a)). Therefore, if the deflection of the EP exceeded the allowable value, it would generate an uneven assembly load on MEA and reduce the performance of the fuel cell. Fig. 21 (b)–(d) show the relationship between the maximum displacement of EP and BPP, the maximum principal stress in the BPP, and the EP thickness. It can be seen that the thicker the EP, the smaller the deformation of EP and BPP, and the more uniform the load distribution. It is worth noting that in addition to the thickness, the structure of the EP also affects the deformation. Lin et al. [42] proposed a multi-objective topology optimisation model for fuel cell EPs. The light weight of the EP is realised and the optimal material distribution is obtained. At the same time, the optimised EP makes the distribution of the assembly load more uniform, which is also convenient for manufacturing. A similar method has been applied to the EP of a fuel cell assembled by a steel strap [125]. Yu et al. [126] proposed a composite sandwich EP made of composite carbon fibre material and composite glass fibre material. The EP has some pre-deformation to obtain a more uniform assembly load distribution. The strength of the EP is comparable to that of a traditional metal EP, while achieving weight reduction. Certain EP design methods have also been proposed to reduce the deformation of the EP and make the assembly load distribution more uniform [127,128].

The conclusions about EP seem to be: 1) The design of EP should maintain good stiffness and achieve lightweight as much as possible; 2) Exploration of more new processes, such as integrated EP integrating the functions of current collector and insulation plate; 3) The appearance of more ingenious assembly mechanisms will change the structure and processing mode of the original EP.

In conclusion, although there have been many meaningful studies on the influence of assembly load on fuel cell components. However, there are also some problems that need further investigation: 1) under different application scenarios and working modes, additional stresses are generated in the fuel cell, such as stresses caused by low temperature start-up, vibration, etc. Therefore, future assembly research should consider more application scenarios and working modes; 2) The aging of fuel cell components is inevitable. In the long-term test process, more work is needed to study whether and how to maintain the good assembly state of each component.

2.2. Effect of assembly load on PEMFC stack performance

Some key parameters of the fuel cell, such as contact resistance, porosity, and gas permeability, are also affected by the assembly load. It is worth noting that the changes in these parameters are closely related to the interaction between fuel cell components, and particularly the interface contact area between the BPP and GDL. Therefore, this part of the review is mainly focussed on fuel cell performance parameters to clarify the impact of the assembly load. Changes in performance parameters affect the transmission of reactants and water and the conduction of electrons, and thereby affect the speed and efficiency of the electrochemical reaction and change the fuel cell output characteristics. Table 2 summarises the relevant studies on stack performance parameters.

According to the current research, the effects of assembly load on water transportation, contact resistance and thermal contact resistance of fuel cell can be clearly evaluated. However, it is difficult to judge the best assembly load according to a certain index in practical application. Therefore, the polarization curve is recommended to evaluate the performance of fuel cells under different assembly loads.

2.2.1. Assembly effect on contact resistance

Reducing the contact resistance can reduce the ohmic loss of fuel cells and prevent the generation of excessive waste heat. Relevant studies show that contact resistance accounts for half of the ohmic loss [147]. In addition to the conversion of hydrogen energy into electric energy through an electrochemical reaction, the remainder of the hydrogen energy is converted into heat through mass transfer and ohmic loss. Therefore, the contact resistance should be reduced as much as possible to reduce heat generation. It has been pointed out that the majority of the contact resistance occurs at the contact interface between the GDL and BPP. With an increase in the assembly load, the contact area of the BPP and GDL increases, and the contact resistance decreases. This is the perspective of current research. The decrease in contact resistance and the increase in contact area further affects the thermal conductivity, which is particularly important for the thermal management of fuel cells.

Table 2
Effect of assembly load on PEMFC stack performance.

Parameter	Relevant conclusions	Reference
Contact resistance	• Reducing CR can reduce power loss and improve fuel cell performance; • CR depends on the assembly load, surface contact state of BPP and GDL, and conductivity and corrosion resistance of the coating; • Increasing assembly load can increase contact surface and reduce CR; • CR decreases nonlinearly with assembly load.	[60,109,111,147, 148,151, 153–155]
Water transportation	• Dynamic balance of water transport is very important for the performance of fuel cells; • Different relative humidity and current density can affect water transport; • Liquid water tends to be transported to the GDL area below the land.	[156,159, 170–177]
Polarization curve	• Under a certain voltage, the current density decreases with the increase of assembly load; • Assembly load mainly affects concentration loss and ohmic loss, but has little effect on activation loss.	[142,178]
Thermal contact resistance	• Thermal contact resistance of fuel cell decreases under assembly load.	[83,179]

Increasing the assembly load can effectively reduce the contact resistance, but excessive interfacial pressure may hinder the transfer of reactants and water discharge, and thus it cannot ensure the improvement of fuel cell performance [148,149]. In order to reduce the contact resistance, Zhou et al. [150] studied the influence of pressure distribution uniformity on the contact resistance under a certain assembly load. They pointed out that when a dimensional error, as shown in Fig. 17, is produced, the contact resistance increases linearly with the accumulation of separation zones. The contact resistance can be reduced by 30% by improving the pressure distribution. Moreover, chemical treatment of the BPP surface to control the microscale irregularities is also helpful in reducing the contact resistance [151–154]. This is more important for metal BPPs. Usually, the graphite BPP has lower contact resistance but higher bulk resistance. The contact area between the BPP and GDL must be increased to reduce the resistance to electron conduction, as shown in Fig. 22. Relevant research shows that 59% of the total power loss is caused by contact resistance [51]. It is noteworthy that coating an MPL on a GDL is also an effective method to reduce surface roughness [26]. Lai et al. [30] pointed out that the contact between the BPP and GDL is the result of coupled mechanical and electrical behaviours. Therefore, an electromechanical FEM was proposed to predict the contact resistance, which solved the limitations of the traditional FEM. Compared with previous methods [109], this method can improve the accuracy of contact resistance prediction and better reflect the electrical behaviour of the contact interface. Moreover, it was found that there is an optimal BPP fillet of 0.6 mm from the perspective of contact resistance optimisation. Mason et al. [129] proposed an in-situ analysis method based on GDL compression displacement and contact resistance. The relationship between the assembly load, compression displacement, and contact

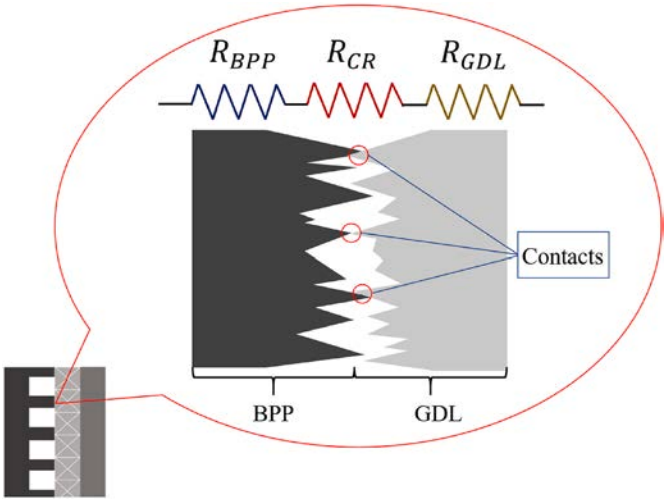

Fig. 22. Relationship between roughness of BPP and contact resistance.

resistance was studied. The results show that an increase in the assembly load leads to a nonlinear decrease in the contact resistance. The inherent contact resistance of different types of GDL is related to its thickness and material. Qiu et al. [155] proposed a microscopic model to predict the contact resistance between the BPP and GDL. The difference between the predicted results and the experimental results was less than 10%.

Although increasing the assembly load can reduce the contact resistance, it does not necessarily help to improve the performance of fuel cells. Therefore, controlling the surface roughness of BPP in contact with GDL is an effective method.

2.2.2. *Assembly effect on water transportation*

Water transport is highly important for the performance of fuel cells. Because protons combine with water molecules and migrate from the anode to the cathode, it is necessary to maintain a certain water content in the membrane to promote proton conduction. Additionally, water produced on the cathode side further increases the water content on the cathode side, thereby forming a concentration gradient [156,157]. Under the action of a concentration gradient, some water diffuses from the cathode side to the anode side. Therefore, water transport in fuel cells is maintained in dynamic equilibrium [158]. A lack of water content lead to a dry membrane, which reduces the proton conductivity of the PEM. If the water content is too high, the GDL pores become blocked and the mass transfer loss increases [159,160]. Therefore, the assembly load should be optimised according to the water content of the MEA.

The problem of water transfer in fuel cells has always been a difficult problem, which is usually accompanied by water and heat management [161,162]. The material composition of the GDL [163,164], porosity [165], material and microstructure of the CL [166,167], the design of the BPP flow field [168,169] and the working conditions of the fuel cell [161] affect water transport. Therefore, the problem of water transmission under an assembly load is not discussed extensively in this review. For further details on water and heat management, please refer to the relevant research.

Cha et al. [170] studied the influence of the assembly load on the water transmission characteristics. The concept of the net drag coefficient is proposed, and the water transmission characteristics under different relative humidity and current densities are compared. As shown in Fig. 23 (a), a positive net drag coefficient indicates that the net water transport occurs in the direction from the anode to the cathode under simultaneous permeation and back diffusion. Fig. 23 (b) shows that the net drag coefficient decreases with an increase in the assembly load and current density at 40% relative humidity. This is due to the increase in osmotic resistance and water back-diffusion [159,171]. In addition, the authors point out that the effect of current density on the net resistance is more significant at low relative humidity. Under the condition of high relative humidity, high assembly load and current density may lead to a change in the water net transmission direction, which should be paid more attention in the design of fuel cells. In addition to transport properties, other studies have shown that the net drag coefficient may also be related to the thickness of the membrane [172,173]. Bazylak et al. [174] observed the transmission path of water in the GDL using an electron microscope and camera. The transmission path of water in the compressed GDL under the optical transparent plate was captured by the microscope. The results show that the preferred path of water transport is the compressed region of the GDL, that is, the GDL region under the rib. This is consistent with the results shown in Fig. 6. This water transport behaviour makes the liquid water easily transported to hard-to-reach areas, which is helpful for the performance of fuel cells. One of the microscopic explanations for this water transport behaviour is that the assembly load leads to the deformation or even damage of fibres in the GDL (Fig. 24), resulting in a large number of hydrophilic and hydrophobic surfaces in the GDL. Water transfer is the result of the combination of water and hydrophilic surfaces in the hydrophobic GDL.

2.2.3. *Assembly effect on polarization curve*

The polarization curve of fuel cell establishes the relationship between output voltage and current, which is the most intuitive standard

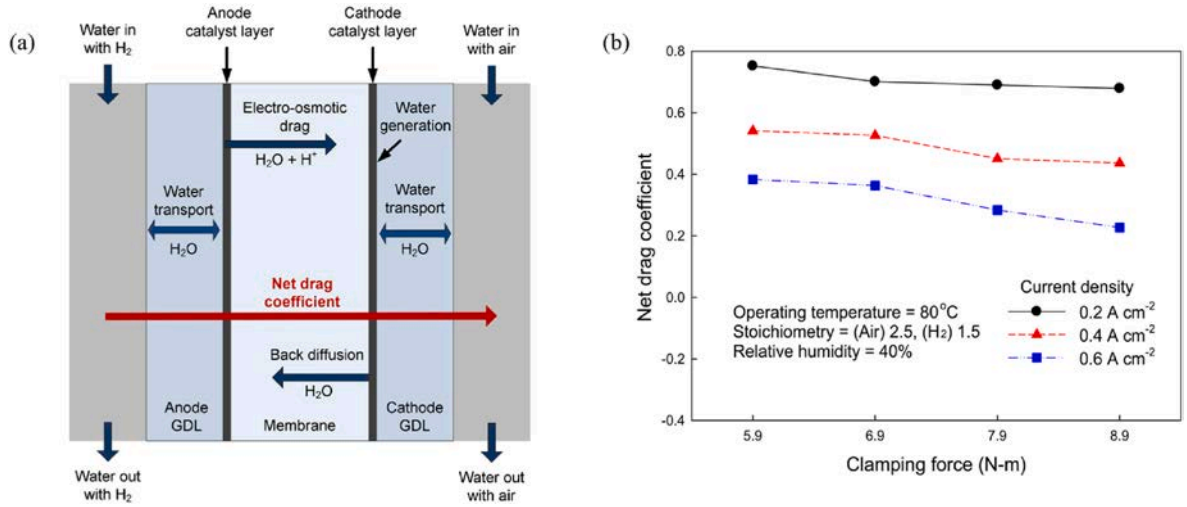

Fig. 23. (a) Definition of net drag coefficient, (b) Relationship between net drag coefficient, current density, and assembly load (relative humidity = 40%) [170].

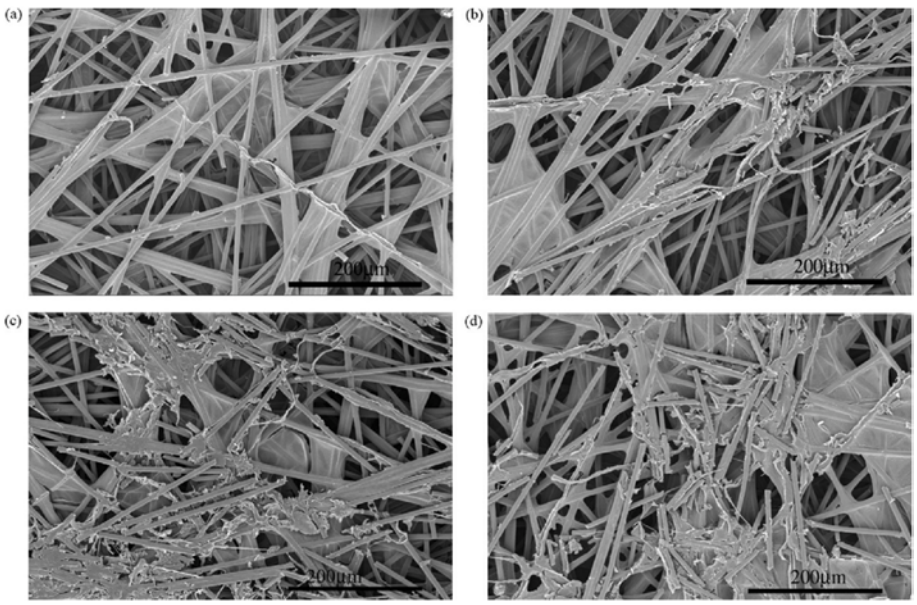

Fig. 24. GDL micrograph under different assembly loads: (a) 0.18 MPa, (b) 0.36 MPa, (c) 0.68 MPa, (d) 1.37 MPa [174].

method to evaluate the performance of fuel cell. Generally, the polarization curve consists of three parts: activation loss, ohmic loss and concentration loss. Lee et al. [178]pointed out that the best fuel cell performance can be found according to the polarization curve of fuel cell under different assembly loads. The typical polarization curve of fuel cell is shown in Fig. 25(a), and the typical polarization curve of fuel cell under different assembly loads is shown in Fig. 25(b). Through the existing research, the following conclusions can be drawn: under a certain voltage, the current density decreases with the increase of assembly load. Assembly load mainly affects concentration loss and ohmic loss, but has little effect on activation loss. This is particularly evident in the research of Toghyani et al. [142]. The possible reason is that the assembly load reduces the thickness of GDL and the space of gas flow in the channel, which is helpful to improve the performance of fuel cell to a certain extent. At the same time, the assembly load reduces the porosity of GDL, so the concentration loss increases especially with the increase of assembly load. It is worth noting that the fuel cell will be permanently damaged under over compression. Therefore, the best assembly load should be found for the fuel cell through the polarization curve before the over compression state is reached.

2.2.4. Assembly effect on thermal contact resistance

During the operation of fuel cell, adjacent components need to transfer heat effectively. The thermal contact resistance is a key parameter of heat transfer. The assembly load also has a certain influence on the thermal contact resistance of fuel cell. Based on the experimental technique of steady-state method, Khandelwal et al. [179] measured the thermal contact resistance between different components of fuel cell. The authors pointed out that the thermal contact resistance between Toray carbon paper and Aluminium bronze decreases with the increase of assembly load. Similar results were found for graphite BPP [83]. That is, the thermal contact resistance between GDL and graphite BPP decreases nonlinearly with the increase of assembly load. During the operation of fuel cell, the heat generated needs to be dissipated outward through the conduction of components. Through relevant research, it can be concluded that the thermal contact resistance of fuel cell decreases under assembly load. The possible reason is that the contact area between components increases and the overall contact resistance decreases.

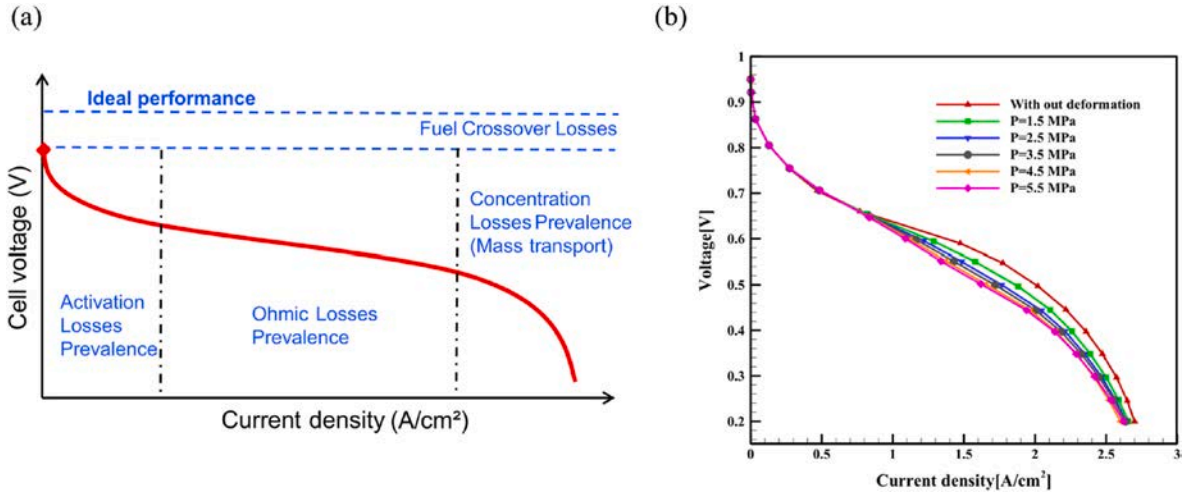

Fig. 25. (a) Typical polarization curve [180], (b) typical polarization curve under different assembly loads [142].

2.3. Effect of assembly load distribution

In addition to the size of the assembly load, the uniform distribution of the assembly load is also an important aspect of assembly technique research. A uniform assembly load can minimise contact resistance and mass transfer loss. However, an uneven assembly load distribution may lead to excessive local thermal resistance, which is not conducive to the consistency of temperature. Moreover, local over-compression may cause reactant blockage, reduce the performance of fuel cells, and even fail to guarantee the tightness of fuel cells. Therefore, assembly load distribution has increasingly been a focus of research in recent years [47, 51,181,182] has begun to increase.

The assembly load is typically realised in three forms: point, line, and surface. In the traditional structural design of a fuel cell stack, the assembly load is applied to the EP by bolts and nuts. Research on this type of assembly load distribution is mainly concerned with the number and distribution of bolts [43,148,181,183]. However, the assembly load distribution of the point load inevitably leads to stress concentration at the edge, as shown in Fig. 9. Therefore, to obtain a more uniform load distribution, a stack structure consisting of a steel strap assembly [125, 184] has gradually appeared in recent years.

Mikkola et al. [185] proposed a general FEM to predict the assembly load distribution under different assembly loads and bolt layouts. A pressure-sensitive film was used to verify the consistency between the predicted and experimental results. Similarly, Alizadeh et al. [47] studied the assembly load distribution on an MEA by combining the FEM and the pressure-sensitive film verification method. It is concluded that the bending of the EP can be reduced to optimise the load distribution by selecting the appropriate EP material and thickness and reducing the bolt torque. Moreover, choosing sealing materials with low hardness and increasing the number of cells can also optimise the assembly load distribution to a certain extent. Other related studies [82,127,150,186] also confirmed the influence of bolt distribution, EP deformation, and seal ring material on the assembly load distribution. In general, the assembly load distribution of the cell in the middle part of the stack is more uniform, especially compared with the cells near the EP. In other words, the cells in the middle of the stack have improved consistency and mechanical states [186]. Usually, the load distribution after an actual assembly can be measured by various experimental methods. Pressure-sensitive films [53,185], piezoresistive sensors [182,187] and carbon paper [181] are commonly used experimental tools.

Through relevant literature research, three conclusions can be drawn for the assembly load distribution: 1) for point load, line load and surface load, generally, surface load can obtain more uniform assembly load distribution; 2) EP is a key factor affecting assembly load distribution. Simply increasing the thickness of the EP can improve the load uniformity. However, the ideal EP design should not reduce the EP stiffness as much as possible and realise lightweight; 3) The ideal assembly load distribution can be obtained by simulation. However, due to the manufacturing accuracy of fuel cell components, the actual assembly load distribution usually deviates from the simulation results. Therefore, more experimental methods can be considered when studying assembly load distribution.

3. Assembly load optimisation

In Section 2, the assembly load and its effect on the fuel cell components were clarified. As one of the important aspects of the assembly technique, the distribution of the assembly load also affects the performance of the fuel cell. Therefore, this section summarises the optimisation of the assembly load. Regarding research content, optimisation research focuses on two important aspects of the assembly technique, namely the assembly load and assembly load distribution. In terms of research methods, simulation methods, experimental methods and analytical methods are the three main techniques to optimise the assembly load. The authors believe that the distribution of assembly load is affected by many factors, so the optimisation of assembly load should be a global optimisation problem. It is difficult to achieve the best effect by simply designing the structure of single element such as EP, MEA and BPP. The literature reviewed in this paper can provide readers with references to the research contents and methods.

3.1. Research content

The optimal design of the assembly load includes two aspects: optimal assembly load and optimal assembly load distribution.

3.1.1. Optimal assembly load

The assembly load is important to the performance of the fuel cell. On one hand, increasing the assembly load can reduce the CR, ohmic loss, and charge transfer resistance, but the porosity of the GDL decreases and the transport resistance of reactants and products increases at the same time. Therefore, the assembly load should not be too large. On the other hand, an insufficient assembly load makes it difficult to meet the basic requirements of stack tightness. Additionally, the assembly load is related to the working conditions of the fuel cell, and the vibration [184], cold start [188,189] and wet thermal stress of the membrane [190,191] change the initial assembly state. Therefore, the optimal assembly load of different stacks should be within a reasonable range.

The equivalent stiffness model (ESM) is a common method in the research of assembly techniques, which is widely used in assembly load design, strength verification, and force analysis of fuel cells [28,184, 192,193]. In the ESM, all the components of the fuel cell are regarded as elastic elements, and all elastic elements form a complete stack through a set of series–parallel relationships. As shown in Fig. 26 (a). The design calculation is carried out on the basis of material mechanics and elastic mechanics, which greatly simplifies the number and difficulty of calculations. Lin et al. [192,193] first proposed the ESM theory and proposed a complete design process for the optimal assembly load. Based on the ESM model, Qiu et al. [28] proposed a design criterion for the optimal assembly load based on CR and GDL porosity. Based on the relationship between porosity and CR with assembly load, the overall expectation function is proposed. Because the two indices of porosity and CR change in opposite directions, the optimal assembly load can be obtained when the overall expectation function is maximised, as shown in Fig. 26 (b). It should be noted that in addition to the two key indicators of CR and porosity, the verification of thermal stress should not be ignored. The assembly load range considering thermal stress may be limited [193], as shown in Fig. 26 (c).

Chen et al. [25] studied the sealing performance and output characteristics of a metal BPP fuel cell under different assembly loads. The torque of the eight bolts was increased from 2 to 7 Nm. The gas leakage rate, polarization curve, and electrochemical impedance spectroscopy of the stack were tested under each assembly load. The experimental results show that gas leakage can be effectively reduced by increasing the assembly load. However, when the bolt torque exceeds 6 Nm, the power of the stack decreases. Based on the experiment, the optimal assembly load is obtained, and it is confirmed that the reduction in power is the joint effect of contact resistance and porosity. Similarly, Al et al. [194] confirmed by in-situ measurements that the performance of a low-temperature fuel cell stack is improved when the assembly load increases from 60 to 150 psi. Yan et al. [82] designed an optimal assembly load based on the characteristics of hydrothermal management under non-uniform GDL compression. The 3D stack model (five-cell liquid-cooled stack) simulates the temperature distribution and molar concentration of oxygen and water in the pressure range of 0.5–3.5. MPa. The polarization curves under different assembly loads show that the highest single-cell output power of 0.65 V can be achieved in the assembly load range of 1.5–3.5. MPa.

From the related research on assembly loads, it can be seen that different stacks have different optimal assembly loads. Increasing the

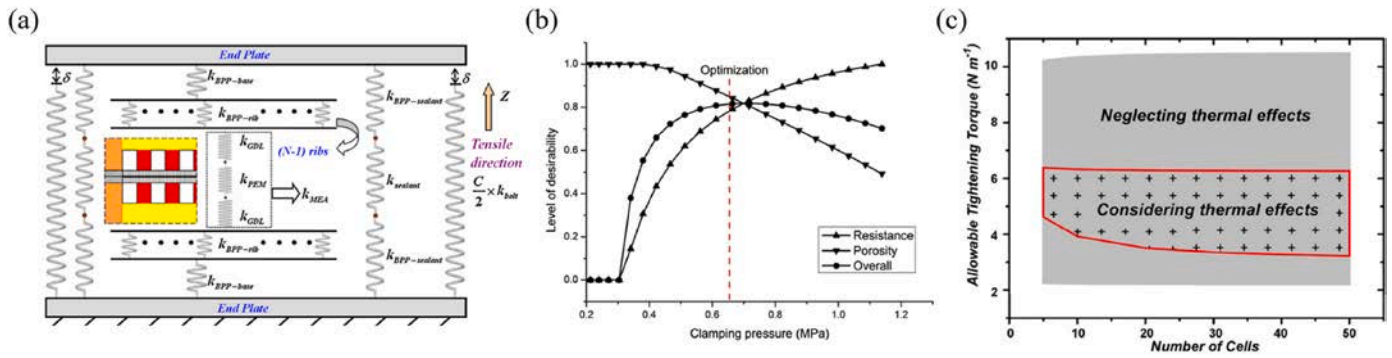

Fig. 26. (a) Equivalent stiffness model [192], (b) Overall expectation function based on CR and GDL porosity [28], (c) Optimal assembly load range considering thermal stress [193].

assembly load improves the stack performance. However, owing to the charge transfer dynamics of the gas reaction rate, the assembly load should not be too large. It should be pointed out that the optimisation of assembly load is only theoretical optimisation. The optimal performance also depends on the uniformity of load distribution to a great extent. In addition, the current literature lacks assembly load optimisation methods for different application scenarios.

3.1.2. Optimal assembly load distribution

Owing to the so-called short plate effect of fuel cells, it is important to maintain a high degree of consistency for improving performance. Here, consistency refers not only to that between cells, but also within a single cell to ensure that the working state of the active region is as uniform as possible. However, for uniformity of the assembly load distribution, the most important aspect is the assembly mechanism. At present, the common research is mainly focused on the bolt and nut assembly structure, and to a lesser degree on the steel strap assembly structure. Other assembly structures such as compliant strap [195], overlapping sheet [196], pneumatic EP [182], and side spring structures [197] are limited to patents. This will be discussed in the next section. For the traditional screw (bolt and nut) assembly, the common consensus is that with an increase in the assembly load, the edge of the MEA will bear more load than the centre, and the inhomogeneity will increase [187].

In experimental research, Montanini et al. [187] combined piezoresistive sensors and digital image technology to optimise the assembly load distribution in the stack. The authors emphasise that there are two key points for the stack of a bolt and nut assembly, which are especially important for the distribution of the assembly load. One of these is the thickness of the EP, and the other is the thickness ratio of the GDL and sealing ring. The authors also suggest that in order to reduce the bending of EPs, pre-bent EPs can be used. In simulation-based research, the results of Bates et al. [53] and Cruz et al. [57] are similar to the experimental results. Some interesting conclusions are put forward: compared with the GDL, the seal ring bears most of the assembly load, and a semi-rigid gasket is recommended to protect the weak part of the MEA edge. From the perspective of optimisation of assembly load distribution, most studies suggest achieving uniform load distribution by optimising the EP, except for the influence of assembly form, bolt number, and layout. First, materials with appropriate strength should be selected, such as aluminium, stainless steel, or non-metallic materials [124,198]. Second, measures to reduce the deformation of the EP should be adopted, such as increasing the thickness [47] or pre-bending [126, 187]. In order to avoid the EP being too bulky, the hydraulic EP [127] and pneumatic EP [51,182] realise more uniform mass transfer by fluid pressure, as shown in Fig. 27.

3.2. Research methods

From the perspective of research methods, these are mainly divided into simulation, experimental and analytical methods.

3.2.1. Simulation methods

In the research on PEMFC assembly, an accurate and effective mathematical model or 3D model can clearly describe basic phenomena in the fuel cell, predict the performance of the stack under different structures and operating conditions, optimise the design and assembly of the fuel cell system, and reduce the production cost. In the research and development of PEMFC assembly techniques, the models have been developed from one dimension to multiple dimensions, from simple to complex. Many researchers have performed extensive simulations, trying to find the best assembly scheme for different PEMFC models.

Zhou et al. [109] established a two-dimensional model of a single cell to explore the change in porosity of the GDL caused by the assembly load and the influence of CR between the GDL and BPP. The authors found an

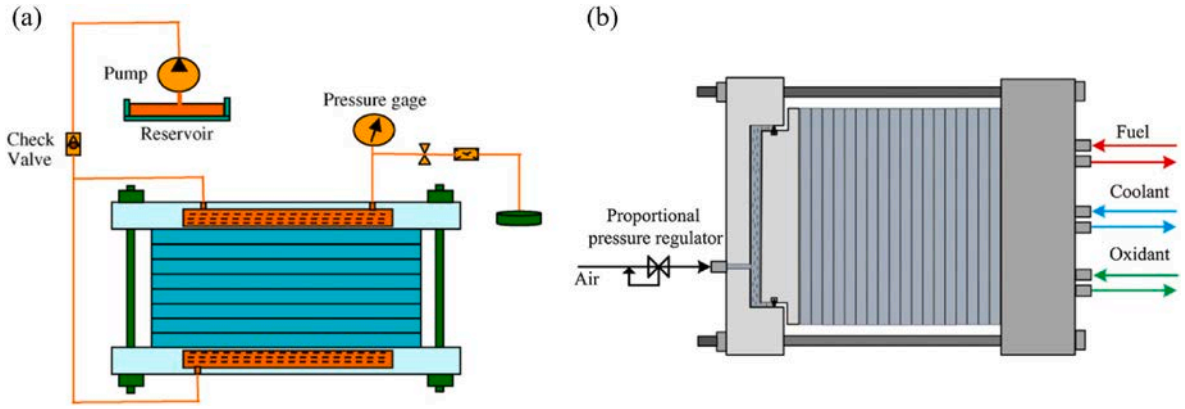

Fig. 27. (a) Hydraulic end plate [127] (b) Pneumatic end plate [182].

optimal BPP rib width, which can obtain a low CR and good porosity of the GDL. Liu et al. [199] established a simplified stack model. A robust design method combining the FEM and response surface methodology (RSM) was used to study the influence of the bolt position and assembly load on the MEA pressure distribution. Lee et al. [34] analysed the uneven stress distribution of the GDL due to the assembly load through a 3D single-cell FEM, and compared it with the stress distribution measured by a pressure sensor in the experiment. Xing et al. [200] used the COMSOL software package to establish a 3D model of a PEMFC to study the influence of the assembly force on the GDL, and used a stochastic algorithm to calculate the optimal assembly load under different voltage conditions. The results showed that when the operating voltage was high, the assembly load of 1–1.5 MPa improved the performance of the fuel cell. Taymaz et al. [201] established a 3D model of a single channel and studied the influence of the assembly load on the GDL. The results show that the CR, porosity, and thickness of the GDL decrease with an increase in the assembly load. The optimal assembly load is between 0.5 and 1 MPa. Perng et al. [202] studied the influence of the interface shape of the reaction gas channel on the performance of a fuel cell by establishing a 3D single-cell model. A trapezoidal cross-section with a slope angle of 60° and a channel height of 1.125 mm is recommended. It can be seen that the research of simulation analysis is mainly focussed on 3D finite element analysis combined with the basic electrochemical principle of fuel cells and mechanical knowledge. However, owing to the complexity of the BPP flow channel, the required number of calculations is too large. Generally, the size of the 3D model is not very large and the number of cells involved is relatively small. At the same time, there are some ideal simplifications and boundary conditions in the model, which yield results of the simulation analysis that are not always satisfactory. It is believed that with the improvement of CPU computing power and speed, this will be improved in the future. It should also be noted that the simulation method usually defaults that the contact between various components is flat. Without considering the influence of tolerance and error, the simulation results are usually different from the experimental results.

3.2.2. Experimental methods

In addition to a wide variety of PEMFC model simulation research, many researchers have also performed numerous experiments to study the impact of assembly on fuel cell performance. In stack assembly experiments, it is usually necessary to apply a certain assembly load with a loading device similar to that in Fig. 3. In addition, the stack assembly machine also has a calibration rod that is convenient for assembly, a pressure plate, a base for uniformly applying assembly force, and certain air-tightness testing equipment. At present, there are many automatic assembly equipment for stacks, but the basic assembly principle and process are similar. During the operation of the press, a series of loading curves are recorded. As mentioned previously, pressure-sensitive techniques are often used in assembly load studies. As shown in Figs. 7 and 9, when the film is loaded with an assembly load, the colour of the film changes. The darker the colour, the greater the load. At the same time, the pressure-sensitive film does not affect the original load distribution [187]. Therefore, pressure-sensitive technologies such as piezoresistive sensors [187] and pressure-sensitive films [43,47,57] are widely used. In addition, 3D image vision technology [187] and microscopy technology [146,174] are also used in the research of assembly loads. Regarding the EP, a coordinate measuring machine (CMM) [186] and stress–strain technology [35] are often used to test its deformation.

3.2.3. Analytical methods

Analytical method is also an important means to study the assembly load of fuel cell. Using the equivalent stiffness model, Lin et al. [192, 193] put forward some valuable analytical equations. For screw assembly stacks, the torque applied to each screw and assembly load can be expressed by Equation (1) and Equation (2).

$$T \quad \frac{F_{clamping}\, d_{eq}}{C} \tag{1}$$

$$d_{eq} \quad \frac{\delta}{2\pi} + \frac{\mu d}{2\cos\beta} + \frac{\mu_n \left(D_1^3 \quad D_0^3\right)}{3\left(D_1^2 \quad D_0^2\right)} \tag{2}$$

where $F_{clamping}$ is the assembly load, T is the torque on each screw, C is the number of screws, d_{eq} is called equivalent frictional diameter. Fig. 28 is a schematic diagram of relevant parameters.

In addition, after considering the air tightness of fuel cell, the strength of MEA and bolt strength, the authors give some analytical equations that can be verified. As shown in Equations (3)–(5). The specific meaning of these analytical equations can be found in Refs. [192,193], which will not be repeated here.

$$\frac{\left(5.5 \times 10^6 + 3.2P_{gas}\right)A_{sealant}}{\sqrt{1000b}} \leq F_{external \quad stack} \leq \zeta \sigma_{sealant}^{yield} A_{sealant} \tag{3}$$

$$F_{internal \quad stack} \leq \gamma \sigma_{PEM}^{yield} A_{rib} \tag{4}$$

$$\sigma_{bolt} \quad \frac{4F_{clamping}}{C\pi d_1^2} \leq \frac{\sigma_{bolt}^{yield}}{n_{safe}} \quad [\sigma_{bolt}] \tag{5}$$

According to the analytical formula in the existing references, when studying the assembly of a specific fuel cell stack, engineers only need to consult the material manual and combine the structure of a specific stack to preliminarily complete the design and verification of the assembly process. In the later stage, further verification by simulation and experimental methods can greatly improve the accuracy of stack assembly design. Therefore, at the beginning of fuel cell assembly design, the efficiency of assembly design can be greatly improved by using analytical method.

4. Assembly mechanism

The assembly load can be provided by point pressure, line pressure, and surface pressure. Therefore, many assembly mechanisms are derived according to different assembly load-holding mechanisms. At present, there are two types of mature stack assembly mechanisms on the market: screw assembly and strap assembly. There is little research on assembly mechanisms in the literature, and most of the work on assembly mechanisms can be found in patents. This section describes the basic assembly mechanisms.

4.1. Screw assembly

The screw assembly is the most popular assembly form on the market, as shown in Fig. 29 (a). The idea of the screw assembly is to convert the point pressure generated by the screw into uniform stress over the whole stack through a thick EP. This method is simple and practical, but the EP occupies a large mass and volume. Moreover, the design of the point load inevitably leads to the assembly load being mainly borne by the edge of the BPP, and the active area of the MEA cannot achieve a uniform assembly load. If the design of the EP is unreasonable, the point load will increase the bending of the EP, which is not conducive to the uniform distribution of the load.

To obtain a more uniform load distribution, screw assembly research mainly involves the optimisation of the EP design. Within this field, it is there is active research on increasing the stiffness without excessively increasing the mass and volume of the EP. This is related to the material selection and the structural design of the EP [203]. Asghari et al. [123] presented a complete development process for an EP, including material selection, finite element analysis, optimal thickness selection, fabrication, and experimental verification. Lin et al. [42] proposed a multi-objective optimisation method for EP design. It not only improves the EP stiffness, but also realises the uniform distribution of the

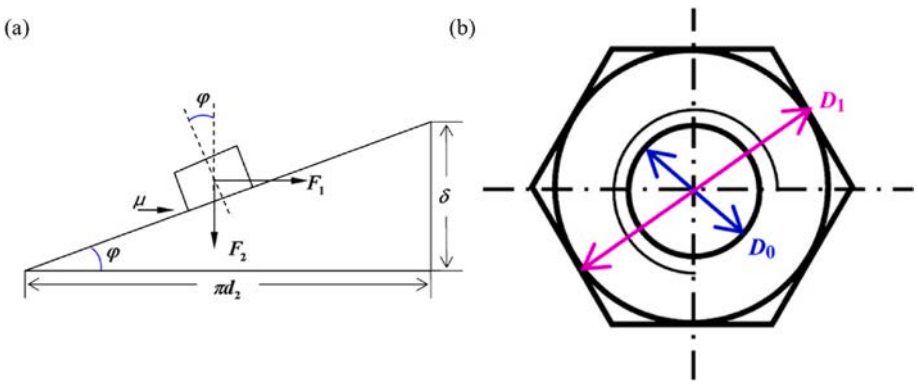

Fig. 28. Schematic diagram of screw assembly: (a) the forces acting on the rectangular thread (b) nut geometry.

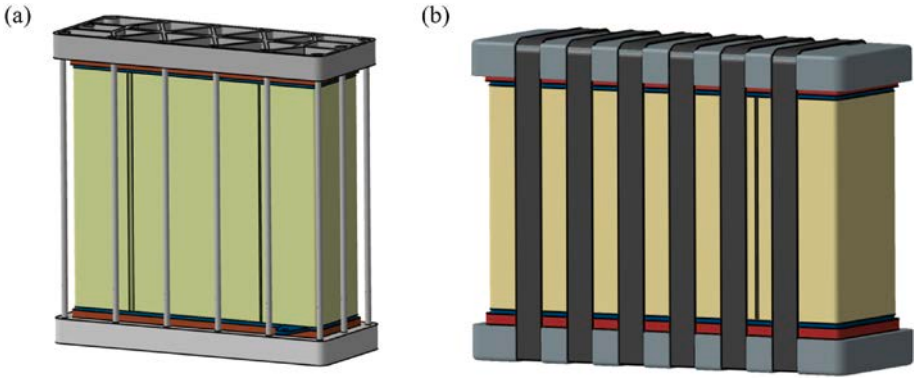

Fig. 29. (a) Screw assembly, (b) Strap assembly.

assembly load. Moreover, the optimised EP structure can meet the machinability and achieve maximum weight reduction. Yu et al. [204] proposed a multi-layer EP structure consisting of a carbon fibre composite and insulation foam. This type of EP can not only maintain the strength, but also reduce the weight and improve the thermal performance. The experimental results show that the design improves the cold start performance of the fuel cell stack.

Pneumatic and hydraulic EPs are also proposed on the basis of screw assembly structures. These two forms apply pressure generated by fluid to the EP without changing the assembly form. As shown in Fig. 27 (b), the concept of a pneumatic EP was proposed by Alizadeh et al. [51]. The reaction gas and coolant flow in and out of the EP on the same side, and the EP on the other side consists of two parts. The inner and outer parts form an air chamber through a sealing ring, which is similar to the piston structure of an engine. The pressure gas pushes the inner EP to realise a uniform distribution of the assembly load. The hydraulic EP has the same operating principle (Fig. 27 (a)). The design of pneumatic and hydraulic EPs improves the load distribution on the active area. The rigidity requirement of the EP is lower, and a lighter structure can be used. At the same time, it allows the assembly load to be monitored for later adjustment [127,182]. However, the complex structure increases the assembly cost.

In terms of patents, Grot et al. [205] proposed the structure of a double-layer upper EP. A number of bolt holes are arranged on the outer layer of the upper EP. By adjusting the screws at different bolt holes, the pressure distribution plate on the inner layer can be controlled to realise a uniform distribution of the assembly load. Toshiyuki et al. [206] also proposed a double-layer EP structure. The EP on one side is composed of internal and external parts, and the two layers are connected by multiple springs. The force of the outer EP is transferred to the inner EP through the spring to achieve a uniform assembly load. The outer EP is connected to the EP on the other side through a screw.

4.2. Strap assembly

The strap assembly is another common assembly structure on the market. Flexible steel straps are commonly used [125]. This method can reduce the thickness and weight of the EP and make the stack more compact. Because of the larger action area of the assembly load, a more uniform load distribution can be obtained [207]. However, the assembly design process of a stack with a strap assembly is more complex. The strap assembly structure is shown in Fig. 29 (b).

Liu et al. [125] designed a semi-circular EP boundary to fit a steel strap. Moreover, the cross-section shape of the EP is lightweight and designed based on the shape optimisation method while ensuring its stiffness. There is also a more typical arc EP with a strap assembly [208]. The characteristic of this stack assembly method is that the EP with a certain radian is used to realise the assembly, which further improves the uniformity of the assembly load. The main advantage is that the upper and lower EPs can adopt certain hollow structures to realise the lightweight design of the stack. However, the EP with a radian is not convenient to use with a press machine. In terms of patents, Boguslaw et al. [209] first proposed the concept of a strap assembly. Unoki et al. [210] connected the two ends of a steel strap with bolts and nuts, and added a strap limiting mechanism on the EP.

4.3. Other stack assembly mechanism

In addition to the above two mainstream stack assembly mechanisms, other assembly mechanisms or improvements to the screw and strap assembly structures can be found through relevant patent searches. Table 3 summarises the assembly mechanisms in patents. These different assembly mechanisms can improve the assembly load distribution to a certain extent. However, the complex mechanical structure makes them difficult to be widely used in commercial stacks. In addition,

Table 3
Assembly mechanism in patent.

No.	Assembly mechanism	Characteristic	Patent No.	Reference
1	Strap	• Adapt to the assembly load variation during operation.	US 2008/0305380 A1	[195]
2	Overlapping sheet	• Prevent relaxation of assembly load.	US 2008/0311457 A1	[196]
3	Side spring	• Keep dynamic assembly load.	US 8012648 B2	[197]
4	Screw	• With assembly load adjusting bolt.	US 6428921 B1	[205]
5	Screw	• Double-layer end plate with spring.	WO 2005/053080 A1	[206]
6	Strap	• With central fluid distributor.	CA 2271706C	[209]
7	Strap	• With strap limiting mechanism.	US 2011/0070520 A1	[210]
8	Strap	• Cross-distribution of compression strap.	WO 2016/205139 A1	[211]
9	Leaf spring	• With tension members.	US 2013/0273452 A1	[212]
10	Tie rod	• Tie rod connects upper and lower end plates.	US 9806369 B2	[213]
11	Coupling mechanism	• Preformed element with a predetermined curvature.	US 9774056 B2	[214]
12	Rigid clamping device	• Define spaces between the end plates.	US 2017/0025701 A1	[215]
13	Tie rod	• Flanges with through holes may receive tie rods.	US 2005/0089737 A1	[216]
14	Rigid frame	• Side Sections integrally formed with the bottom.	US 6218039 B1	[217]
15	Fastening housing	• Housing equipped with a load adjusting device.	US 6670069 B2	[218]
16	Strap	• The strap forms a closed circuit.	US 2006/0093890 A1	[219]
17	Screw	• Multiple fuel cell sub-stacks disposed in parallel.	US 5945232	[220]
18	Strap	• Use disc spring end plate.	US 5993987	[221]
19	Screw	• Use element for reducing stress concentration.	US 2006/0240307 A1	[222]
20	Tension bar	• The tension bars have a certain angle of inclination.	US 2014/0162168 A1	[223]
21	Compression shell	• The upper and lower shells are interlocked.	US 2014/0255818 A1	[224]
22	Fixed carriage	• Fuel cells can be built directly in the carriage.	US 7435501 B2	[225]
23	Screw	• Liquid-filled sealed receptacles are under end plates.	EP 0936689 B1	[226]
24	Screw	• Pressure bellows are under end plates.	EP 1284521 A2	[227]
25	Screw	• Two-phase fluid bladder are under end plates.	US 6200698 B1	[228]
26	Planar strip	• Counteract the strain caused by MEA expansion.	US 2008/0145713 A1	[229]
27	Tie rod	• Spring assembly is horizontally below the end plate.	US 6413665 B1	[230]
28	Screw	• Spring plate is below the end plate.	US 6372372 B1	[231]

there is a lack of comparative analysis of the assembly mechanisms involved in the patent to more clearly point out the applicable working scenarios of each assembly mechanism.

5. Automatic assembly

At present, the biggest obstacles to the commercialisation of fuel cells are their high cost and durability [232]. The cost of fuel cell stacks can be divided into three parts: material and component cost, labour cost (i.e. design, manufacturing, and assembly), and capital cost of manufacturing equipment. Owing to the wide use of precious metals in fuel cell components, the cost of materials and components is largely independent of economies of scale. Technological innovation is effective in reducing the cost of materials and components. However, the improvement of automation and large-scale production can effectively reduce labour and capital costs, which can theoretically reduce the cost of stacks by 50% [233]. The ultimate goal of the U.S. Department of Energy (DoE) is to reduce the cost of fuel cell stack to \$15/kW_{net} through technological innovation and mass production practices [234]. As a significant part of production, increasing the assembly efficiency is important for reducing the cost of fuel cells.

The basic assembly process of the fuel cell is as follows: (1) the BPP, MEA, and BPP are superimposed on the lower EP in sequence (the insulation plate and current collector have been installed) to assemble the first single cell; (2) the above step is repeated and single cells are stacked by using the assembly auxiliary positioning device; (3) after the final single cell is installed, the upper EP and other components are stacked; (4) air tightness test; (5) after passing the tightness test, the screw is installed (assembly force-holding device) while maintaining the pressure. At present, some fuel cell stacks undergo a long manual assembly process, which involves repeated work cycles, and human errors are inevitable. A stack assembled by hand may require a whole day to complete the assembly and testing process. In the fuel cell development cycle, the early prototype stacks can be manually assembled. However, with large-scale production, it is necessary to ensure the reliability and consistency of stack quality. With a large number of applications of PEMFC stacks in automobiles, the increase in power and volume of fuel cell stacks means an increase in the number of single cells. For the repeated work cycle in the assembly process, subjective and objective factors related to the quality of products and workers should be minimised. Moreover, the requirement of assembly speed further proves the rationality of using an automatic assembly processes. At present, with the automatic manufacturing of fuel cell components, the automation of the assembly process is increasingly important [235].

Fig. 30 shows the complete stack automation assembly process. It includes three processes: component feed, stack assembly, and press. The assembly automation production line needs expansibility while ensuring high efficiency. High efficiency refers to the requirements of incoming feed speed and beat, and the traceability of incoming materials is also required. The expansibility should not only meet the assembly capability for different types of stacks (such as graphite and metal BPPs), but also consider the requirements of modular expansion for the entire production line, such as adding an automatic assembly module for components and a stack test module.

Automatic assembly is getting more and more widely used, but it also faces a series of difficulties and challenges. The first is the alignment accuracy of the manipulator. Owing to the flexibility and mobility problems caused by the multi-joint structure of the manipulator, the alignment accuracy is limited [237]. Traditional manual assembly usually uses alignment pins to constraint the relationship between components. During the operation of the manipulator, the use of alignment pins may cause jamming in the component placement process, especially for soft structures such as MEAs. However, the alignment process without alignment pins potentially suffers from low alignment accuracy. Low alignment accuracy makes it impossible to meet the designed constraint relationship between components, resulting in gas leakage and other problems. The second is the design of the end effector of the manipulator. The components of a fuel cell composed of different materials have different stiffness; for example, BPPs have higher stiffness while MEAs are softer. The end effector requires the ability to

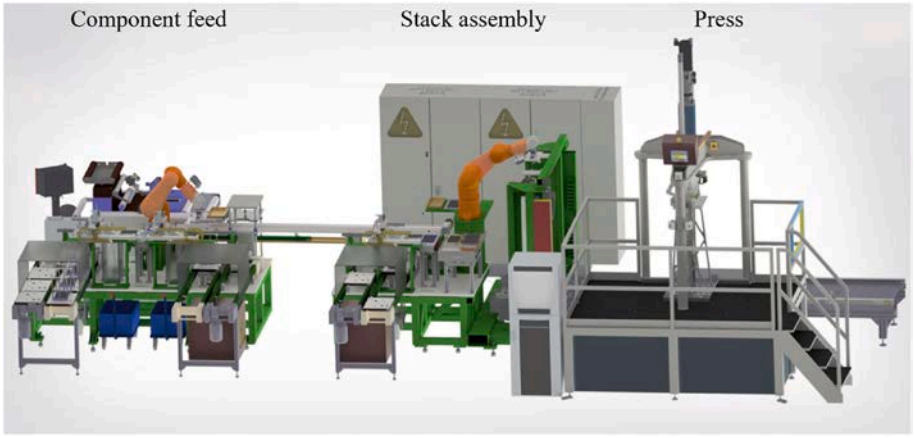

Fig. 30. Complete stack automation assembly process [236].

control these different components to ensure stability and accuracy in the process of picking and releasing [238]. However, using too many manipulators and end effectors would greatly increase the complexity and cost of the automatic production line. The final difficulty is the integration of the fuel cell design and assembly process. At present, the design and assembly of fuel cells are usually divided into two different processes. In the design process of a fuel cell, the demand for automatic assembly is seldom considered, which leads to a series of unexpected problems such as alignment and picking difficulty.

Therefore, it can be concluded that the development of a complete automated stack assembly line should meet the following basic requirements: (1) precision and repetitive precision control, (2) automatic incoming components, (3) flexibility in handling different types of components, (4) scalability, and (5) traceability of products and components.

Laskowski et al. [239,240] designed an assembly automation production line of a PEMFC stack with three robot working units, and found that the existing stack structure has many disadvantages for automation. Based on the relevant knowledge of the product design and assembly criteria [241], the authors analysed the parts that can be improved in the assembly process, re-optimised the stack, shortened the assembly time, and improved the assembly efficiency. It can be seen that the design and assembly of fuel cells should be combined. In production, engineers should build a complete fault mode characterisation system to quickly find the source of the fault, accurately implement quality control, and reduce the probability of repeated assembly and testing.

Manual assembly often uses alignment pins to ensure the assembly accuracy of components. However, in automatic assembly, repeated insertion and extraction of alignment pins would be detrimental to the balance and accuracy of assembly. To solve this problem, Williams et al. [242] used a manipulator to align non-conductive alignment pins. The end of the alignment pin is conical, which facilitates the release process of the components, and can be permanently retained in the stack after assembly. In the following study [238], the authors optimised the original end effector. The new end effector can pick up and release different components using a vacuum cup. Moreover, a passive compliance system is added to compensate for the limitation of the manipulator's mobility, and to mitigate possible jamming problems caused by components falling along the alignment pins. Fig. 31 shows the picking and releasing processes of the manipulator. In addition, optimising the stack assembly process, reducing the number of assembly steps, and reducing the complexity of the assembly system are also significant for improving the efficiency of automatic assembly [243–247].

In the automatic assembly process, the new design of some fuel cells will change the assembly process. For example, Honda's fuel cell unit is

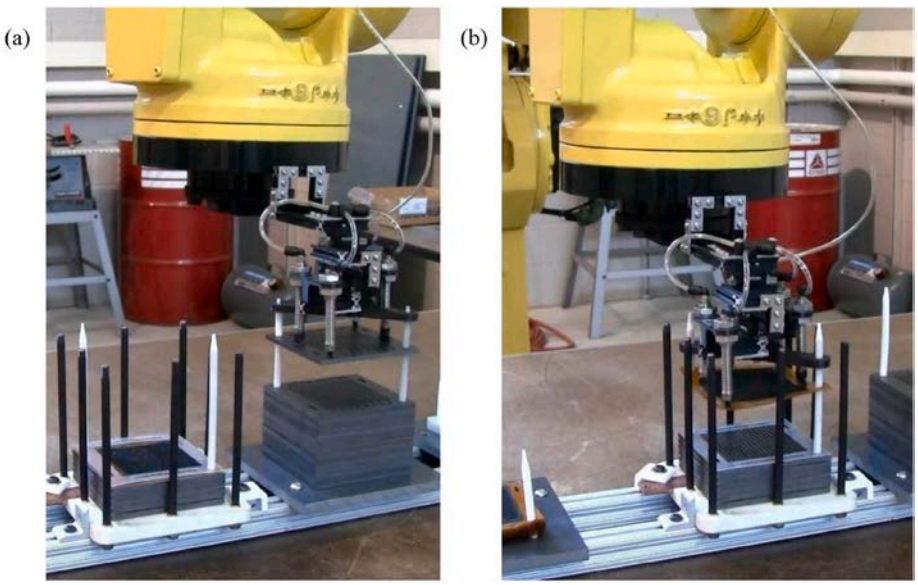

Fig. 31. Picking and releasing process of the manipulator: (a) picking BPP, (b) releasing MEA [238].

composed of two MEAs and three separators [248,249]. As shown in Fig. 32 (a). This structure can effectively protect MEA, because MEA does not need to be operated separately in the assembly process. Therefore, in the assembly process, the manipulator only needs to operate the pre-assembled fuel cell unit. As shown in Fig. 32 (b). This improves the assembly efficiency and simplifies the manipulator end effector to a certain extent. In addition, a structure which can be connected with the connection bar is designed around the fuel cell unit. After the stack is assembled, each fuel cell unit is fixed with the connection bar. Both ends of the connection bar are respectively fixed on the upper and lower EP. This design can effectively prevent the dislocation caused by vibration during the use of the stack. As shown in Fig. 32 (c). Integrated assembly technique is used in the fuel cell assembly process of AA Allied Power Technologies Ltd. (APT) [250]. Twelve fuel cell single cells were first assembled into Xell™ module (output power of 3.6 kW). The Xell™ module can be assembled into a stack according to the power demand. The power range covers 10 kW–120 kW. As shown in Fig. 33 (a). This integrated assembly technique has strong scalability. Due to the prior assembly into separate Xell™ modules, the assembly accuracy of each module can be well controlled, and the overall assembly accuracy of the stack is also improved. In addition, a horizontal servo stack assembly machine has been developed, which adopts horizontal assembly mode to reduce the influence of gravity. As shown in Fig. 33 (b).

It can be seen that automated fuel cell stack assembly requires complex system engineering. The process involves the design and manufacture of fuel cells, the development and supply of fuel cell components, the design of the automation process, and the manufacturing, testing, and maintenance of an automatic production line [251]. Then, the product design, design of fuel cell components to meet the requirements of automation-oriented manufacturing, assembly, and testing are required. Then, there is the construction of a complete automated production line, including component supply, assembly, and compression processes. Finally, equipment testing and prototype stack manufacturing are carried out to verify the rationality of the entire process and improve it.

6. Summary/conclusions

This review summarises the research on assembly techniques from four aspects: assembly load, assembly load optimisation, assembly mechanism, and automatic assembly. Assembly load is an important aspect of stack assembly design. The influence of the assembly load on the components and the distribution of the assembly load affect the output performance of the stack. Section 2 summarises related research on assembly load. After understanding the mechanism of assembly load, researchers optimise the assembly load and its distribution through a series of experimental, analytical and simulation-based methods, hoping to obtain the best performance of the fuel cell. These points are referred to in Section 3. After a thorough review of the literature and published patents, Section 4 summarises the different stack assembly mechanisms. Section 5 introduces automatic stack assembly from the perspective of improving assembly efficiency and reducing stack cost, which is also a current focal point of active assembly research.

The purpose of this paper is to summarise the research and progress of assembly techniques and provide a reference for researchers and engineers who study PEMFC stack assembly. It can be seen from the summary of the full text that assembly is a systematic technique oriented by production which closely combines with theoretical and practical aspects. The development of assembly techniques can not only promote theoretical research, such as the mechanical properties of key components and mass transfer of fuel cells, but also guide the production process, improve production efficiency, and promote large-scale application of fuel cells. The main conclusions and research directions are as follows:

(1) At present, great progress has been made in the research on the influence of assembly load on the mechanism and performance of fuel cell. Through various analytical methods, simulation and experimental methods, the best assembly load and its distribution can be obtained. However, in the actual operation of fuel cell, other stresses will appear in the fuel cell. Such as thermal stress caused by uneven temperature, stress caused by vibration and low temperature start-up. The relationship between assembly load and these stresses and the effect of their combination are not clear. Therefore, in the future research process of assembly technique, the influence of these stresses generated in the actual operation process should be considered more.

(2) The current research methods of assembly technique (simulation method, experimental method and analytical method) are carried out in the off-line state of fuel cell, that is, when the fuel cell is not running. However, the components of fuel cell will be aged during operation, such as the decrease of seal ring thickness. How to detect the assembly state of fuel cell under on-line condition and design a mechanism that can dynamically adjust the assembly load is the future research direction.

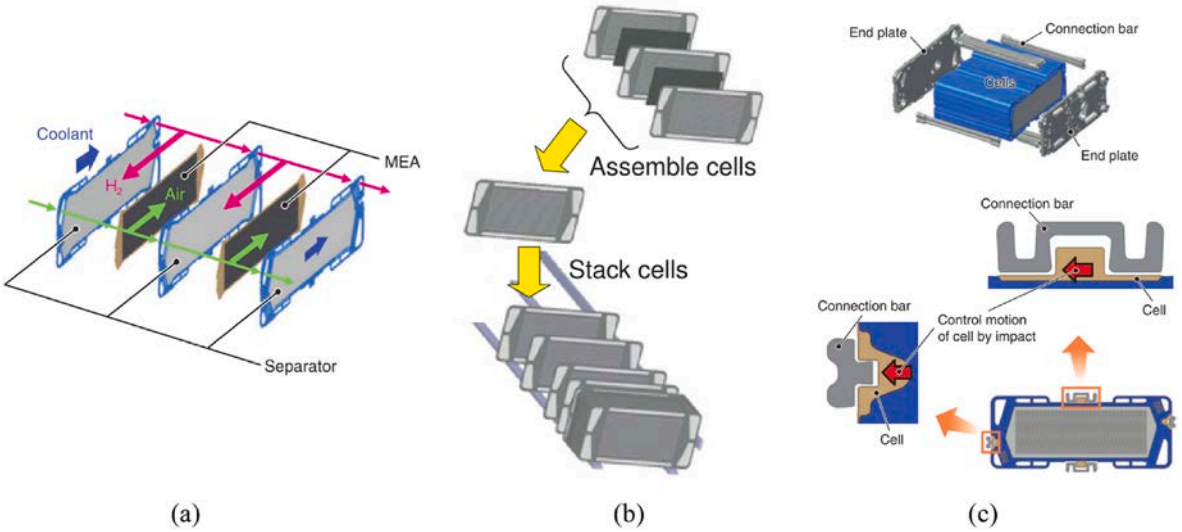

Fig. 32. Honda FC stack: (a) FC unit with 2 MEAs and 3 separators, (b) stack assembly, (c) connection bar with high impact resistance [248,249].

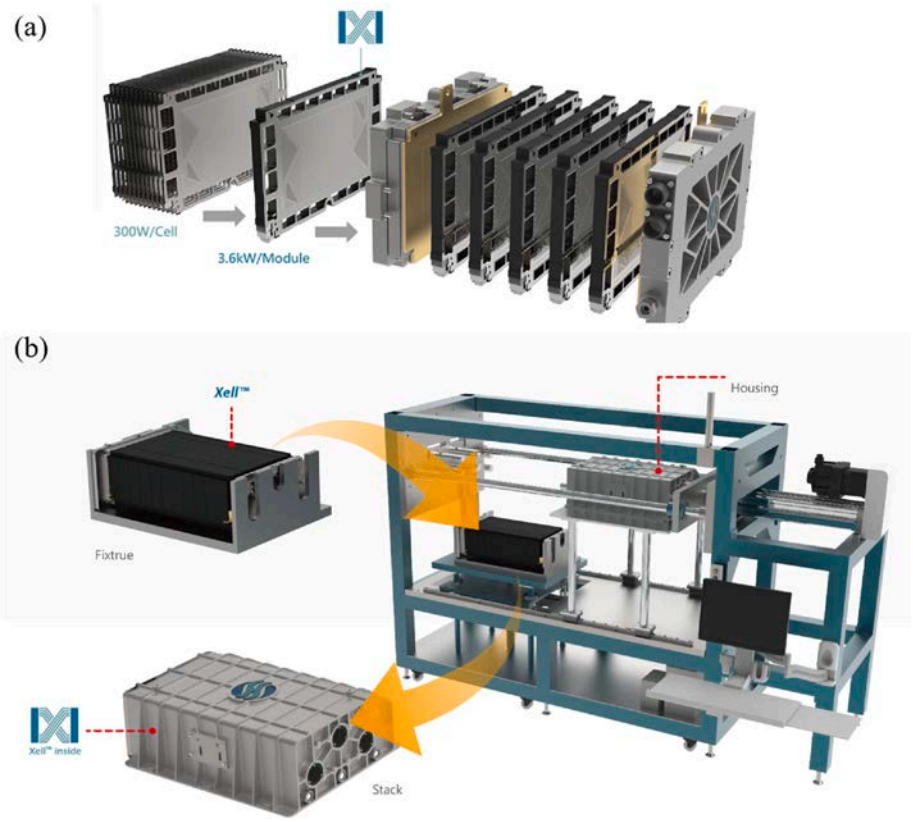

Fig. 33. Integrated assembly technique: (a) Xell™ Inside stack, (b) horizontal servo stack assembly machine [250].

(3) Although there are many novel fuel cell assembly mechanisms in the patent literature, the real market-oriented assembly mechanisms are still screw assembly and strap assembly. Therefore, more research is needed to compare and analyse the advantages and disadvantages of different assembly mechanisms. In the future, the assembly mechanism with lower cost and better effect should be selected according to different application scenarios of fuel cell.
(4) It is certain that automatic assembly is the development direction of assembly technique in the future. In this regard, there seem to be two feasible development paths. First, pay attention to the optimisation of the manipulator end effector, so that it can operate more objects and be more accurate and flexible. The second is to consider the convenience of assembly at the beginning of the design of fuel cell. More ingenious fuel cell component design can greatly simplify the assembly process and improve efficiency. At this point, the authors have more confidence in the development of the latter.
(5) Design, manufacturing and assembly are the key factors to ensure the performance of fuel cell and reduce the cost. In fact, the three processes are strongly coupled. Although a series of progress has been made in the development of assembly technique, assembly technique is still limited by the manufacturing accuracy of fuel cell components and the defects at the beginning of fuel cell design. Further improving the assembly effect (such as load distribution uniformity and assembly efficiency) is facing the challenge of fuel cell design and manufacturing. Therefore, future research should better coordinate the three aspects of design, manufacturing and assembly.

Therefore, the authors think that the next stage of research on assembly techniques will continue to focus on theory and practice. In theory, the assembly load will be studied deeply, and the mechanical and performance changes in the fuel cell during the assembly process will be thoroughly understood. On this basis, a reasonable assembly load and appropriate assembly mechanism will be designed for the stack. In practice, the two processes of fuel cell design and assembly design are unified to design fuel cell components from the perspective of improving assembly efficiency. The theoretical research is taken as guidance for the fuel cell design and assembly process. With the improvement of assembly techniques, there is an urgent need to construct unified assembly processes, standards, and specifications in the industry. The development of fuel cell assembly techniques will greatly promote the industrialisation of PEMFCs, reduce stack manufacturing costs, and realise the wider application of fuel cells in diverse fields.

Declaration of competing interest

The authors declare that they have no known competing financial interests or personal relationships that could have appeared to influence the work reported in this paper.

Acknowledgement

This work is financially supported by the National Key R&D Program of China (No. 2017YFE0101400), Anhui Provincial Development and Reform Commission Project (No. KZ0170020190568) and the National Natural Science Foundation of China (Grant No. 52072265).

References

[1] Musa SD, Zhonghua T, Ibrahim AO, Habib M. China's energy status: a critical look at fossils and renewable options. Renew Sustain Energy Rev 2018;81:2281–90. https://doi.org/10.1016/j.rser.2017.06.036.
[2] Martins F, Felgueiras C, Smitková M. Fossil fuel energy consumption in European countries. Energy Procedia 2018;153:107–11. https://doi.org/10.1016/j.egypro.2018.10.050.

[3] Chen Z-M, Chen P-L, Ma Z, Xu S, Hayat T, Alsaedi A. Inflationary and distributional effects of fossil energy price fluctuation on the Chinese economy. Energy 2019;187:115974. https://doi.org/10.1016/j.energy.2019.115974.

[4] Lu Y, Li H, Lu C, Wu K, Chen Z, Wang K, et al. The effect of completion strategy on fracture propagation from multiple cluster perforations in fossil hydrogen energy development. Int J Hydrogen Energy 2019;44:7168–80. https://doi.org/10.1016/j.ijhydene.2019.01.121.

[5] Chang K, Ye Z, Wang W. Volatility spillover effect and dynamic correlation between regional emissions allowances and fossil energy markets: new evidence from China's emissions trading scheme pilots. Energy 2019;185:1314–24. https://doi.org/10.1016/j.energy.2019.07.132.

[6] Rath BN, Akram V, Bal DP, Mahalik MK. Do fossil fuel and renewable energy consumption affect total factor productivity growth? Evidence from cross-country data with policy insights. Energy Pol 2019;127:186–99. https://doi.org/10.1016/j.enpol.2018.12.014.

[7] Wang ZX, Ye DJ. Forecasting Chinese carbon emissions from fossil energy consumption using non-linear grey multivariable models. J Clean Prod 2017;142:600–12. https://doi.org/10.1016/j.jclepro.2016.08.067.

[8] Thomas G, Pidgeon N, Roberts E. Ambivalence, naturalness and normality in public perceptions of carbon capture and storage in biomass, fossil energy, and industrial applications in the United Kingdom. Energy Research and Social Science 2018;46:1–9. https://doi.org/10.1016/j.erss.2018.06.007.

[9] Curtin J, McInerney C, Ó Gallachóir B, Hickey C, Deane P, Deeney P. Quantifying stranding risk for fossil fuel assets and implications for renewable energy investment: a review of the literature. Renew Sustain Energy Rev 2019;116:109402. https://doi.org/10.1016/j.rser.2019.109402.

[10] Tsai BH, Chang CJ, Chang CH. Elucidating the consumption and CO2 emissions of fossil fuels and low-carbon energy in the United States using Lotka-Volterra models. Energy 2016;100:416–24. https://doi.org/10.1016/j.energy.2015.12.045.

[11] Nguyen TLT, Hermansen JE, Mogensen L. Fossil energy and GHG saving potentials of pig farming in the EU. Energy Pol 2010;38:2561–71. https://doi.org/10.1016/j.enpol.2009.12.051.

[12] Cho JH, Sohn SY. A novel decomposition analysis of green patent applications for the evaluation of R&D efforts to reduce CO 2 emissions from fossil fuel energy consumption. J Clean Prod 2018;193:290–9. https://doi.org/10.1016/j.jclepro.2018.05.060.

[13] Gabrielli P, Poluzzi A, Kramer GJ, Spiers C, Mazzotti M, Gazzani M. Seasonal energy storage for zero-emissions multi-energy systems via underground hydrogen storage. Renew Sustain Energy Rev 2020;121:109629. https://doi.org/10.1016/j.rser.2019.109629.

[14] Hanley ES, Deane JP, Gallachóir BPÓ. The role of hydrogen in low carbon energy futures–A review of existing perspectives. Renew Sustain Energy Rev 2018;82:3027–45. https://doi.org/10.1016/j.rser.2017.10.034.

[15] Parra D, Valverde L, Pino FJ, Patel MK. A review on the role, cost and value of hydrogen energy systems for deep decarbonisation. Renew Sustain Energy Rev 2019;101:279–94. https://doi.org/10.1016/j.rser.2018.11.010.

[16] Liu S, Chen T, Zhang C, Xie Y. Study on the performance of proton exchange membrane fuel cell (PEMFC) with dead-ended anode in gravity environment. Appl Energy 2020;261:114454. https://doi.org/10.1016/j.apenergy.2019.114454.

[17] Peng F, Ren L, Zhao Y, Li L. Hybrid dynamic modeling-based membrane hydration analysis for the commercial high-power integrated PEMFC systems considering water transport equivalent. Energy Convers Manag 2020;205:112385. https://doi.org/10.1016/j.enconman.2019.112385.

[18] Serra PMD, Espírito-Santo A, Magrinho M. A steady-state electrical model of a microbial fuel cell through multiple-cycle polarization curves. Renew Sustain Energy Rev 2020;117:109439. https://doi.org/10.1016/j.rser.2019.109439.

[19] Baroutaji A, Wilberforce T, Ramadan M, Olabi AG. Comprehensive investigation on hydrogen and fuel cell technology in the aviation and aerospace sectors. Renew Sustain Energy Rev 2019;106:31–40. https://doi.org/10.1016/j.rser.2019.02.022.

[20] Gittleman CS, Kongkanand A, Masten D, Gu W. Materials research and development focus areas for low cost automotive proton-exchange membrane fuel cells. Current Opinion in Electrochemistry 2019;18:81–9. https://doi.org/10.1016/j.coelec.2019.10.009.

[21] Qiu D, Peng L, Lai X, Ni M, Lehnert W. Mechanical failure and mitigation strategies for the membrane in a proton exchange membrane fuel cell. Renew Sustain Energy Rev 2019;113:109289. https://doi.org/10.1016/j.rser.2019.109289.

[22] Arsalis A. A comprehensive review of fuel cell-based micro-combined-heat-and-power systems. Renew Sustain Energy Rev 2019;105:391–414. https://doi.org/10.1016/j.rser.2019.02.013.

[23] Priya K, Sathishkumar K, Rajasekar N. A comprehensive review on parameter estimation techniques for Proton Exchange Membrane fuel cell modelling. Renew Sustain Energy Rev 2018;93:121–44. https://doi.org/10.1016/j.rser.2018.05.017.

[24] Dafalla AM, Jiang F. Stresses and their impacts on proton exchange membrane fuel cells: a review. Int J Hydrogen Energy 2018;43:2327–48. https://doi.org/10.1016/j.ijhydene.2017.12.033.

[25] Chen CY, Su SC. Effects of assembly torque on a proton exchange membrane fuel cell with stamped metallic bipolar plates. Energy 2018;159:440–7. https://doi.org/10.1016/j.energy.2018.06.168.

[26] Guerrero Moreno N, Cisneros Molina M, Gervasio D, Pérez Robles JF. Approaches to polymer electrolyte membrane fuel cells (PEMFCs) and their cost. Renew Sustain Energy Rev 2015. https://doi.org/10.1016/j.rser.2015.07.157.

[27] Raza R, Akram N, Javed MS, Rafique A, Ullah K, Ali A, et al. Fuel cell technology for sustainable development in Pakistan - an over-view. Renew Sustain Energy Rev 2016;53:450–61. https://doi.org/10.1016/j.rser.2015.08.049.

[28] Qiu D, Yi P, Peng L, Lai X. Assembly design of proton exchange membrane fuel cell stack with stamped metallic bipolar plates. Int J Hydrogen Energy 2015. https://doi.org/10.1016/j.ijhydene.2015.03.064.

[29] Giacoppo G, Hovland S, Barbera O. 2 kW Modular PEM fuel cell stack for space applications: development and test for operation under relevant conditions. Appl Energy 2019;242:1683–96. https://doi.org/10.1016/j.apenergy.2019.03.188.

[30] Lai X, Liu D, Peng L, Ni J. A mechanical-electrical finite element method model for predicting contact resistance between bipolar plate and gas diffusion layer in PEM fuel cells. J Power Sources 2008;182:153–9. https://doi.org/10.1016/j.jpowsour.2008.03.069.

[31] Zhou Y, Lin G, Shih AJ, Hu SJ. A micro-scale model for predicting contact resistance between bipolar plate and gas diffusion layer in PEM fuel cells. J Power Sources 2007;163:777–83. https://doi.org/10.1016/j.jpowsour.2006.09.019.

[32] Shahgaldi S, Ozden A, Li X, Hamdullahpur F. A novel membrane electrode assembly design for proton exchange membrane fuel cells: characterization and performance evaluation. Electrochim Acta 2019;299:809–19. https://doi.org/10.1016/j.electacta.2019.01.064.

[33] Wu Z, Zhou Y, Lin G, Wang S, Hu SJ. An improved model for predicting electrical contact resistance between bipolar plate and gas diffusion layer in proton exchange membrane fuel cells. J Power Sources 2008. https://doi.org/10.1016/j.jpowsour.2008.03.044.

[34] Lee SJ, Hsu C De, Huang CH. Analyses of the fuel cell stack assembly pressure. J Power Sources 2005;145:353–61. https://doi.org/10.1016/j.jpowsour.2005.02.057.

[35] Carral C, Mélé P. A numerical analysis of PEMFC stack assembly through a 3D finite element model. Int J Hydrogen Energy 2014. https://doi.org/10.1016/j.ijhydene.2014.01.036.

[36] Su ZY, Liu CT, Chang HP, Li CH, Huang KJ, Sui PC. A numerical investigation of the effects of compression force on PEM fuel cell performance. J Power Sources 2008. https://doi.org/10.1016/j.jpowsour.2008.04.060.

[37] Carral C, Charvin N, Trouvé H, Mélé P. An experimental analysis of PEMFC stack assembly using strain gage sensors. Int J Hydrogen Energy 2014;39:4493–501. https://doi.org/10.1016/j.ijhydene.2014.01.033.

[38] Ozden A, Shahgaldi S, Li X, Hamdullahpur F. A review of gas diffusion layers for proton exchange membrane fuel cells—with a focus on characteristics, characterization techniques, materials and designs. Prog Energy Combust Sci 2019;74:50–102. https://doi.org/10.1016/j.pecs.2019.05.002.

[39] De las Heras A, Vivas FJ, Segura F, Andújar JM. From the cell to the stack. A chronological walk through the techniques to manufacture the PEFCs core. Renew Sustain Energy Rev 2018;96:29–45. https://doi.org/10.1016/j.rser.2018.07.036.

[40] Khetabi EM, Bouziane K, Zamel N, François X, Meyer Y, Candusso D. Effects of mechanical compression on the performance of polymer electrolyte fuel cells and analysis through in-situ characterisation techniques - a review. J Power Sources 2019;424:8–26. https://doi.org/10.1016/j.jpowsour.2019.03.071.

[41] Bograchev D, Gueguen M, Grandidier JC, Martemianov S. Stress and plastic deformation of MEA in running fuel cell. Int J Hydrogen Energy 2008;33:5703–17. https://doi.org/10.1016/j.ijhydene.2008.06.066.

[42] Lin P, Zhou P, Wu CW. Multi-objective topology optimization of end plates of proton exchange membrane fuel cell stacks. J Power Sources 2011;196:1222–8. https://doi.org/10.1016/j.jpowsour.2010.08.072.

[43] Wen CY, Lin YS, Lu CH. Experimental study of clamping effects on the performances of a single proton exchange membrane fuel cell and a 10-cell stack. J Power Sources 2009;192:475–85. https://doi.org/10.1016/j.jpowsour.2009.03.058.

[44] Ous T, Arcoumanis C. Effect of compressive force on the performance of a proton exchange membrane fuel cell. J Mech Eng Sci 2007;221. https://doi.org/10.1243/09544062JMES654.

[45] Movahedi M, Ramiar A, Ranjber AA. 3D numerical investigation of clamping pressure effect on the performance of proton exchange membrane fuel cell with interdigitated flow field. Energy 2018;142:617–32. https://doi.org/10.1016/j.energy.2017.10.020.

[46] Charon W, Iltchev MC, Blachot JF. Mechanical simulation of a Proton Exchange Membrane Fuel Cell stack using representative elementary volumes of stamped metallic bipolar plates. Int J Hydrogen Energy 2014;39:13195–205. https://doi.org/10.1016/j.ijhydene.2014.06.125.

[47] Alizadeh E, Barzegari MM, Momenifar M, Ghadimi M, Saadat SHM. Investigation of contact pressure distribution over the active area of PEM fuel cell stack. Int J Hydrogen Energy 2016;41:3062–71. https://doi.org/10.1016/j.ijhydene.2015.12.057.

[48] Millichamp J, Mason TJ, Neville TP, Rajalakshmi N, Jervis R, Shearing PR, et al. Mechanisms and effects of mechanical compression and dimensional change in polymer electrolyte fuel cells - a review. J Power Sources 2015;284:305–20. https://doi.org/10.1016/j.jpowsour.2015.02.111.

[49] Fekrazad N, Bergman TL. The effect of compressive load on proton exchange membrane fuel cell stack performance and behavior. J Heat Tran 2007. https://doi.org/10.1115/1.2728909.

[50] Zhang L, Liu Y, Song H, Wang S, Zhou Y, Hu SJ. Estimation of contact resistance in proton exchange membrane fuel cells. J Power Sources 2006;162:1165–71. https://doi.org/10.1016/j.jpowsour.2006.07.070.

[51] Alizadeh E, Ghadimi M, Barzegari MM, Momenifar M, Saadat SHM. Development of contact pressure distribution of PEM fuel cell's MEA using novel clamping

mechanism. Energy 2017;131:92–7. https://doi.org/10.1016/j.energy.2017.05.036.
[52] Hartnig C, Manke I, Kuhn R, Kleinau S, Goebbels J, Banhart J. High-resolution in-plane investigation of the water evolution and transport in PEM fuel cells. J Power Sources 2009;188:468–74. https://doi.org/10.1016/j.jpowsour.2008.12.023.
[53] Bates A, Mukherjee S, Hwang S, Lee SC, Kwon O, Choi GH, et al. Simulation and experimental analysis of the clamping pressure distribution in a PEM fuel cell stack. Int J Hydrogen Energy 2013;38:6481–93. https://doi.org/10.1016/j.ijhydene.2013.03.049.
[54] Xiao Y, Cho C. Experimental investigation and discussion on the mechanical endurance limit of nafion membrane used in proton exchange membrane fuel cell. Energies 2014;7:6401–11. https://doi.org/10.3390/en7106401.
[55] Gatto I, Urbani F, Giacoppo G, Barbera O, Passalacqua E. Influence of the bolt torque on PEFC performance with different gasket materials. Int J Hydrogen Energy 2011. https://doi.org/10.1016/j.ijhydene.2011.07.066.
[56] Zhou Y, Lin G, Shih AJ, Hu SJ. Assembly pressure and membrane swelling in PEM fuel cells. J Power Sources 2009;192:544–51. https://doi.org/10.1016/j.jpowsour.2009.01.085.
[57] de la Cruz J, Cano U, Romero T. Simulation and in situ measurement of stress distribution in a polymer electrolyte membrane fuel cell stack. J Power Sources 2016;329:273–80. https://doi.org/10.1016/j.jpowsour.2016.08.073.
[58] Bograchev D, Gueguen M, Grandidier JC, Martemianov S. Stress and plastic deformation of MEA in fuel cells. Stresses generated during cell assembly. J Power Sources 2008;180:393–401. https://doi.org/10.1016/j.jpowsour.2008.02.048.
[59] Khatib FN, Wilberforce T, Ijaodola O, Ogungbemi E, El-Hassan Z, Durrant A, et al. Material degradation of components in polymer electrolyte membrane (PEM) electrolytic cell and mitigation mechanisms: a review. Renew Sustain Energy Rev 2019;111:1–14. https://doi.org/10.1016/j.rser.2019.05.007.
[60] Sadeghifar H. In-plane and through-plane electrical conductivities and contact resistances of a Mercedes-Benz catalyst-coated membrane, gas diffusion and micro-porous layers and a Ballard graphite bipolar plate: impact of humidity, compressive load and polytetrafluoroe. Energy Convers Manag 2017;154:191–202. https://doi.org/10.1016/j.enconman.2017.10.060.
[61] Ismail MS, Damjanovic T, Ingham DB, Pourkashanian M, Westwood A. Effect of polytetrafluoroethylene-treatment and microporous layer-coating on the electrical conductivity of gas diffusion layers used in proton exchange membrane fuel cells. J Power Sources 2010;195:2700–8. https://doi.org/10.1016/j.jpowsour.2009.11.069.
[62] Qiu D, Peng L, Liang P, Yi P, Lai X. Mechanical degradation of proton exchange membrane along the MEA frame in proton exchange membrane fuel cells. Energy 2018;165:210–22. https://doi.org/10.1016/j.energy.2018.09.136.
[63] Chun JH, Jo DH, Kim SG, Park SH, Lee CH, Kim SH. Improvement of the mechanical durability of micro porous layer in a proton exchange membrane fuel cell by elimination of surface cracks. Renew Energy 2012;48:35–41. https://doi.org/10.1016/j.renene.2012.04.011.
[64] Li Y, Dillard DA, Lai YH, Case SW, Ellis MW, Budinski MK, et al. Experimental measurement of stress and strain in nafion membrane during hydration cycles. J Electrochem Soc 2012;159. https://doi.org/10.1149/2.065202jes.
[65] Vengatesan S, Fowler MW, Yuan XZ, Wang H. Diagnosis of MEA degradation under accelerated relative humidity cycling. J Power Sources 2011;196:5045–52. https://doi.org/10.1016/j.jpowsour.2011.01.088.
[66] Khattra NS, Karlsson AM, Santare MH, Walsh P, Busby FC. Effect of time-dependent material properties on the mechanical behavior of PFSA membranes subjected to humidity cycling. J Power Sources 2012;214:365–76. https://doi.org/10.1016/j.jpowsour.2012.04.065.
[67] Solasi R, Zou Y, Huang X, Reifsnider K, Condit D. On mechanical behavior and in-plane modeling of constrained PEM fuel cell membranes subjected to hydration and temperature cycles. J Power Sources 2007;167:366–77. https://doi.org/10.1016/j.jpowsour.2007.02.025.
[68] Poornesh KK, Cho CD, Lee GB, Tak YS. Gradation of mechanical properties in gas-diffusion electrode. Part 2: heterogeneous carbon fiber and damage evolution in cell layers. J Power Sources 2010;195:2718–30. https://doi.org/10.1016/j.jpowsour.2009.11.030.
[69] Malekian A, Salari S, Tam M, Djilali N, Bahrami M. Compressive behaviour of thin catalyst layers. Part II - model development and validation. Int J Hydrogen Energy 2019;44:18461–71. https://doi.org/10.1016/j.ijhydene.2019.04.135.
[70] Park K, Ohnishi T, Goto M, So M, Takenaka S, Tsuge Y, et al. Improvement of cell performance in catalyst layers with silica-coated Pt/carbon catalysts for polymer electrolyte fuel cells. Int J Hydrogen Energy 2019;45:1867–77. https://doi.org/10.1016/j.ijhydene.2019.11.097.
[71] Malekian A, Salari S, Stumper J, Djilali N, Bahrami M. Effect of compression on pore size distribution and porosity of PEM fuel cell catalyst layers. Int J Hydrogen Energy 2019;44:23396–405. https://doi.org/10.1016/j.ijhydene.2019.07.036.
[72] Rong F, Huang C, Liu ZS, Song D, Wang Q. Microstructure changes in the catalyst layers of PEM fuel cells induced by load cycling. Part II. Simulation and understanding. J Power Sources 2008;175:712–23. https://doi.org/10.1016/j.jpowsour.2007.10.007.
[73] Ma L, Liu ZS, Huang C, Chen SH, Meng GW. Microstructure changes induced by capillary condensation in catalyst layers of PEM fuel cells. Int J Hydrogen Energy 2010;35:12182–90. https://doi.org/10.1016/j.ijhydene.2010.08.072.
[74] Uchiyama T, Kumei H, Yoshida T. Catalyst layer cracks by buckling deformation of membrane electrode assemblies under humidity cycles and mitigation methods. J Power Sources 2013;238:403–12. https://doi.org/10.1016/j.jpowsour.2013.04.026.
[75] Li W, Lin R, Yang Y. One simple method to mitigate the structure degradation of alloy catalyst layer in PEMFC. Electrochim Acta 2019;323:134823. https://doi.org/10.1016/J.ELECTACTA.2019.134823.
[76] Kaneko T, Yoshimoto Y, Hori T, Takagi S, Ooyama J, Terao T, et al. Relation between oxygen gas diffusivity and porous characteristics under capillary condensation of water in cathode catalyst layers of polymer electrolyte membrane fuel cells. Int J Heat Mass Tran 2020;150. https://doi.org/10.1016/j.ijheatmasstransfer.2019.119277.
[77] Litster S, McLean G. PEM fuel cell electrodes. J Power Sources 2004;130:61–76. https://doi.org/10.1016/j.jpowsour.2003.12.055.
[78] Malekian A, Salari S, Tam M, Oldknow K, Djilali N, Bahrami M. Compressive behaviour of thin catalyst layers. Part I - experimental study. Int J Hydrogen Energy 2019;44:18450–60. https://doi.org/10.1016/j.ijhydene.2019.04.134.
[79] Kim S, Ahn BK, Mench MM. Physical degradation of membrane electrode assemblies undergoing freeze/thaw cycling: diffusion media effects. J Power Sources 2008;179:140–6. https://doi.org/10.1016/j.jpowsour.2007.12.114.
[80] Lee SY, Lee KS, Um S. The structural variation of the gas diffusion layer and a performance evaluation of polymer electrolyte fuel cells as a function of clamping pressure. J Mech Sci Technol 2008;22:565–74. https://doi.org/10.1007/s12206-007-1211-6.
[81] Chi PH, Chan SH, Weng FB, Su A, Sui PC, Djilali N. On the effects of non-uniform property distribution due to compression in the gas diffusion layer of a PEMFC. Int J Hydrogen Energy 2010;35:2936–48. https://doi.org/10.1016/j.ijhydene.2009.05.066.
[82] Yan X, Lin C, Zheng Z, Chen J, Wei G, Zhang J. Effect of clamping pressure on liquid-cooled PEMFC stack performance considering inhomogeneous gas diffusion layer compression. Appl Energy 2020;258:114073. https://doi.org/10.1016/j.apenergy.2019.114073.
[83] Nitta I, Himanen O, Mikkola M. Thermal conductivity and contact resistance of compressed gas diffusion layer of PEM fuel cell. Fuel Cell 2008. https://doi.org/10.1002/fuce.200700054.
[84] Ismail MS, Hassanpour A, Ingham DB, Ma L, Pourkashanian M. On the compressibility of gas diffusion layers in proton exchange membrane fuel cells. Fuel Cell 2012;12:391–7. https://doi.org/10.1002/fuce.201100054.
[85] Kleemann J, Finsterwalder F, Tillmetz W. Characterisation of mechanical behaviour and coupled electrical properties of polymer electrolyte membrane fuel cell gas diffusion layers. J Power Sources 2009;190:92–102. https://doi.org/10.1016/j.jpowsour.2008.09.026.
[86] Norouzifard V, Bahrami M. Deformation of PEM fuel cell gas diffusion layers under compressive loading: an analytical approach. J Power Sources 2014;264:92–9. https://doi.org/10.1016/j.jpowsour.2014.04.057.
[87] Senthil Velan V, Velayutham G, Rajalakshmi N, Dhathathreyan KS. Influence of compressive stress on the pore structure of carbon cloth based gas diffusion layer investigated by capillary flow porometry. Int J Hydrogen Energy 2014;39:1752–9. https://doi.org/10.1016/j.ijhydene.2013.11.038.
[88] Gaiselmann G, Totzke C, Manke I, Lehnert W, Schmidt V. 3D microstructure modeling of compressed fiber-based materials. J Power Sources 2014;257:52–64. https://doi.org/10.1016/j.jpowsour.2014.01.095.
[89] James JP, Choi HW, Pharoah JG. X-ray computed tomography reconstruction and analysis of polymer electrolyte membrane fuel cell porous transport layers. Int J Hydrogen Energy 2012;37:18216–30. https://doi.org/10.1016/j.ijhydene.2012.08.077.
[90] Kim AR, Jung HM, Um S. An engineering approach to optimal metallic bipolar plate designs reflecting gas diffusion layer compression effects. Energy 2014;66:50–5. https://doi.org/10.1016/j.energy.2013.08.009.
[91] El-kharouf A, Steinberger-Wilckens R. The effect of clamping pressure on gas diffusion layer performance in polymer electrolyte fuel cells. Fuel Cell 2015;15:802–12. https://doi.org/10.1002/fuce.201500088.
[92] Tanaka S, Bradfield WW, Legrand C, Malan AG. Numerical and experimental study of the effects of the electrical resistance and diffusivity under clamping pressure on the performance of a metallic gas-diffusion layer in polymer electrolyte fuel cells. J Power Sources 2016;330:273–84. https://doi.org/10.1016/j.jpowsour.2016.08.121.
[93] El-Kharouf A, Rees NV, Steinberger-Wilckens R. Gas diffusion layer materials and their effect on polymer electrolyte fuel cell performance – ex situ and in situ characterization. Fuel Cell 2014;14:735–41. https://doi.org/10.1002/fuce.201300247.
[94] Zhou Y, Jiao K, Du Q, Yin Y, Li X. Gas diffusion layer deformation and its effect on the transport characteristics and performance of proton exchange membrane fuel cell. Int J Hydrogen Energy 2013;38:12891–903. https://doi.org/10.1016/j.ijhydene.2013.05.150.
[95] Serincan MF, Pasaogullari U. Effect of gas diffusion layer anisotropy on mechanical stresses in a polymer electrolyte membrane. J Power Sources 2011;196:1314–20. https://doi.org/10.1016/j.jpowsour.2010.06.026.
[96] Fadzillah DM, Rosli MI, Talib MZM, Kamarudin SK, Daud WRW. Review on microstructure modelling of a gas diffusion layer for proton exchange membrane fuel cells. Renew Sustain Energy Rev 2017;77:1001–9. https://doi.org/10.1016/j.rser.2016.11.235.
[97] Patel V, Battrell L, Anderson R, Zhu N, Zhang L. Investigating effect of different gas diffusion layers on water droplet characteristics for proton exchange membrane (PEM) fuel cells. Int J Hydrogen Energy 2019;44:18340–50. https://doi.org/10.1016/j.ijhydene.2019.05.111.
[98] Liu D, Peng L, Lai X. Effect of dimensional error of metallic bipolar plate on the GDL pressure distribution in the PEM fuel cell. Int J Hydrogen Energy 2009;34:990–7. https://doi.org/10.1016/j.ijhydene.2008.10.081.

[99] Qiu D, Yi P, Peng L, Lai X. Study on shape error effect of metallic bipolar plate on the GDL contact pressure distribution in proton exchange membrane fuel cell. Int J Hydrogen Energy 2013;38:6762–72. https://doi.org/10.1016/j.ijhydene.2013.03.105.
[100] Hottinen T, Himanen O. PEMFC temperature distribution caused by inhomogeneous compression of. GDL 2007;9:1047–52. https://doi.org/10.1016/j.elecom.2006.12.018.
[101] Wilberforce T, El Hassan Z, Ogungbemi E, Ijaodola O, Khatib FN, Durrant A, et al. A comprehensive study of the effect of bipolar plate (BP) geometry design on the performance of proton exchange membrane (PEM) fuel cells. Renew Sustain Energy Rev 2019;111:236–60. https://doi.org/10.1016/j.rser.2019.04.081.
[102] Song Y, Zhang C, Ling CY, Han M, Yong RY, Sun D, et al. Review on current research of materials, fabrication and application for bipolar plate in proton exchange membrane fuel cell. Int J Hydrogen Energy 2019. https://doi.org/10.1016/j.ijhydene.2019.07.231.
[103] Peng L, Yi P, Lai X. Design and manufacturing of stainless steel bipolar plates for proton exchange membrane fuel cells. Int J Hydrogen Energy 2014;39:21127–53. https://doi.org/10.1016/j.ijhydene.2014.08.113.
[104] García-Salaberri PA, Vera M, Zaera R. Nonlinear orthotropic model of the inhomogeneous assembly compression of PEM fuel cell gas diffusion layers. Int J Hydrogen Energy 2011;36:11856–70. https://doi.org/10.1016/j.ijhydene.2011.05.152.
[105] Ciavarella M, Hills DA, Monno G. Influence of rounded edges on indentation by a flat punch. Proc IME C J Mech Eng Sci 1998;212:319–28.
[106] Nitta I, Hottinen T, Himanen O, Mikkola M. Inhomogeneous compression of PEMFC gas diffusion layer. Part I. Experimental. J Power Sources 2007;171:26–36. https://doi.org/10.1016/j.jpowsour.2006.11.018.
[107] Hottinen T, Himanen O, Karvonen S, Nitta I. Inhomogeneous compression of PEMFC gas diffusion layer. Part II. Modeling the effect. J Power Sources 2007;171:113–21. https://doi.org/10.1016/j.jpowsour.2006.10.076.
[108] Uchiyama T, Kato M, Yoshida T. Buckling deformation of polymer electrolyte membrane and membrane electrode assembly under humidity cycles. J Power Sources 2012;206:37–46. https://doi.org/10.1016/j.jpowsour.2012.01.073.
[109] Zhou P, Wu CW, Ma GJ. Contact resistance prediction and structure optimization of bipolar plates. J Power Sources 2006;159:1115–22. https://doi.org/10.1016/j.jpowsour.2005.12.080.
[110] Matsuura T, Kato M, Hori M. Study on metallic bipolar plate for proton exchange membrane fuel cell. J Power Sources 2006;161:74–8. https://doi.org/10.1016/j.jpowsour.2006.04.064.
[111] Sadeghifar H, Djilali N, Bahrami M. Thermal conductivity of a graphite bipolar plate (BPP) and its thermal contact resistance with fuel cell gas diffusion layers: effect of compression, PTFE, micro porous layer (MPL), BPP out-of-flatness and cyclic load. J Power Sources 2015;273:96–104. https://doi.org/10.1016/j.jpowsour.2014.09.062.
[112] Wang H, Sweikart MA, Turner JA. Stainless steel as bipolar plate material for polymer electrolyte membrane fuel cells. J Power Sources 2003;115:243–51. https://doi.org/10.1016/S0378-7753(03)00023-5.
[113] Mishra V, Yang F, Pitchumani R. Measurement and prediction of electrical contact resistance between gas diffusion layers and bipolar plate for applications to PEM fuel cells. J Fuel Cell Sci Technol 2004;1:2–9. https://doi.org/10.1115/1.1782917.
[114] Mishra V, Yang F, Pitchumani R. Analysis and design of PEM fuel cells. J Power Sources 2005;141:47–64. https://doi.org/10.1016/j.jpowsour.2004.08.051.
[115] Deng D, Murakawa H. FEM prediction of buckling distortion induced by welding in thin plate panel structures. Comput Mater Sci 2008;43:591–607. https://doi.org/10.1016/j.commatsci.2008.01.003.
[116] Taherian R. A review of composite and metallic bipolar plates in proton exchange membrane fuel cell: materials, fabrication, and material selection. J Power Sources 2014;265:370–90. https://doi.org/10.1016/j.jpowsour.2014.04.081.
[117] Ye DH, Zhan ZG. A review on the sealing structures of membrane electrode assembly of proton exchange membrane fuel cells. J Power Sources 2013;231:285–92. https://doi.org/10.1016/j.jpowsour.2013.01.009.
[118] Tan J, Chao YJ, Li X, Zee JW Van. Degradation of silicone rubber under compression in a simulated. PEM fuel cell environment 2007;172:782–9. https://doi.org/10.1016/j.jpowsour.2007.05.026.
[119] Tan J, Chao YJ, Yang M, Lee WK, Van Zee JW. Chemical and mechanical stability of a Silicone gasket material exposed to PEM fuel cell environment. Int J Hydrogen Energy 2011;36:1846–52. https://doi.org/10.1016/j.ijhydene.2009.12.048.
[120] Lin CW, Chien CH, Tan J, Chao YJ, Van Zee JW. Chemical degradation of five elastomeric seal materials in a simulated and an accelerated PEM fuel cell environment. J Power Sources 2011;196:1955–66. https://doi.org/10.1016/j.jpowsour.2010.10.012.
[121] Lin CW, Chien CH, Tan J, Chao YJ, Van Zee JW. Dynamic mechanical characteristics of five elastomeric gasket materials aged in a simulated and an accelerated PEM fuel cell environment. Int J Hydrogen Energy 2011;36:6756–67. https://doi.org/10.1016/j.ijhydene.2011.02.112.
[122] Cleghorn SJC, Mayfield DK, Moore DA, Moore JC, Rusch G, Sherman TW, et al. A polymer electrolyte fuel cell life test : 3 years of continuous operation 2006;158:446–54. https://doi.org/10.1016/j.jpowsour.2005.09.062.
[123] Asghari S, Shahsamandi MH, Ashraf Khorasani MR. Design and manufacturing of end plates of a 5 kW PEM fuel cell. Int J Hydrogen Energy 2010;35:9291–7. https://doi.org/10.1016/j.ijhydene.2010.02.135.
[124] Kim JS, Park J Bin, Kim YM, Ahn SH, Sun HY, Kim KH, et al. Fuel cell end plates: a review. Int J Precis Eng Manuf 2008;9(1):39–46.
[125] Liu B, Wei MY, Ma GJ, Zhang W, Wu CW. Stepwise optimization of endplate of fuel cell stack assembled by steel belts. Int J Hydrogen Energy 2016;41:2911–8. https://doi.org/10.1016/j.ijhydene.2015.12.047.
[126] Yu HN, Kim SS, Suh J Do, Lee DG. Composite endplates with pre-curvature for PEMFC (polymer electrolyte membrane fuel cell). Compos Struct 2010;92:1498–503. https://doi.org/10.1016/j.compstruct.2009.10.023.
[127] Wang X, Song Y, Zhang B. Experimental study on clamping pressure distribution in PEM fuel cells. J Power Sources 2008;179:305–9. https://doi.org/10.1016/j.jpowsour.2007.12.055.
[128] Karvonen S, Hottinen T, Ihonen J, Uusalo H. Modeling of polymer electrolyte membrane fuel cell stack end plates. J Fuel Cell Sci Technol (USA) n.d. 2016;5.041009–1.
[129] Mason TJ, Millichamp J, Neville TP, El-Kharouf A, Pollet BG, Brett DJL. Effect of clamping pressure on ohmic resistance and compression of gas diffusion layers for polymer electrolyte fuel cells. J Power Sources 2012;219:52–9. https://doi.org/10.1016/j.jpowsour.2012.07.021.
[130] Aldakheel F, Ismail MS, Hughes KJ, Ingham DB, Ma L, Pourkashanian M. Effects of compression on mechanical integrity, gas permeability and thermal stability of gas diffusion layers with/without sealing gaskets. Int J Hydrogen Energy 2021;46:22907–19. https://doi.org/10.1016/j.ijhydene.2021.04.087.
[131] Omrani R, Shabani B. Gas diffusion layer modifications and treatments for improving the performance of proton exchange membrane fuel cells and electrolysers: a review. Int J Hydrogen Energy 2017;42:28515–36. https://doi.org/10.1016/j.ijhydene.2017.09.132.
[132] Ramani D, Khattra NS, Singh Y, Mohseni-Javid A, Orfino FP, Dutta M, et al. Mitigation of mechanical membrane degradation in fuel cells – Part 1: gas diffusion layers with low surface roughness. J Power Sources 2021:230446. doi:10.1016/j.jpowsour.2021.230446.
[133] Kim GH, Kim D, Kim J, Kim H, Park T. Impact of cracked gas diffusion layer on performance of polymer electrolyte membrane fuel cells. J Ind Eng Chem 2020;91:311–6. https://doi.org/10.1016/j.jiec.2020.08.014.
[134] Kanchan BK, Randive P, Pati S. Numerical investigation of multi-layered porosity in the gas diffusion layer on the performance of a PEM fuel cell. Int J Hydrogen Energy 2020. https://doi.org/10.1016/j.ijhydene.2020.05.218.
[135] Kang DG, Lee DK, Choi JM, Shin DK, Kim MS. Study on the metal foam flow field with porosity gradient in the polymer electrolyte membrane fuel cell. Renew Energy 2020;156:931–41. https://doi.org/10.1016/j.renene.2020.04.142.
[136] Benziger J, Kimball E, Mejia-Ariza R, Kevrekidis I. Oxygen mass transport limitations at the cathode of polymer electrolyte membrane fuel cells. AIChE J 2011. https://doi.org/10.1002/aic.12455.
[137] Turkmen AC, Celik C. The effect of different gas diffusion layer porosity on proton exchange membrane fuel cells. Fuel 2018;222:465–74. https://doi.org/10.1016/j.fuel.2018.02.058.
[138] Akiki T, Charon W, Iltchev MC, Accary G, Kouta R. Influence of local porosity and local permeability on the performances of a polymer electrolyte membrane fuel cell. J Power Sources 2010;195:5258–68. https://doi.org/10.1016/j.jpowsour.2010.03.020.
[139] Mukherjee M, Bonnet C, Lapicque F. Estimation of through-plane and in-plane gas permeability across gas diffusion layers (GDLs): comparison with equivalent permeability in bipolar plates and relation to fuel cell performance. Int J Hydrogen Energy 2020;45:13428–40. https://doi.org/10.1016/j.ijhydene.2020.03.026.
[140] Chien CH, Hu YL, Su TH, Liu HT, Wang CT, Yang PF, et al. Effects of bolt pre-loading variations on performance of GDL in a bolted PEMFC by 3-D FEM analysis. Energy 2016;113:1174–87. https://doi.org/10.1016/j.energy.2016.07.075.
[141] Banerjee R, Hinebaugh J, Liu H, Yip R, Ge N, Bazylak A. Heterogeneous porosity distributions of polymer electrolyte membrane fuel cell gas diffusion layer materials with rib-channel compression. Int J Hydrogen Energy 2016;41:14885–96. https://doi.org/10.1016/j.ijhydene.2016.06.147.
[142] Toghyani S, Moradi Nafchi F, Afshari E, Hasanpour K, Baniasadi E, Atyabi SA. Thermal and electrochemical performance analysis of a proton exchange membrane fuel cell under assembly pressure on gas diffusion layer. Int J Hydrogen Energy 2018;43:4534–45. https://doi.org/10.1016/j.ijhydene.2018.01.068.
[143] Li S, Sundén B. Effects of gas diffusion layer deformation on the transport phenomena and performance of PEM fuel cells with interdigitated flow fields. Int J Hydrogen Energy 2018;43:16279–92. https://doi.org/10.1016/j.ijhydene.2018.07.064.
[144] Li WZ, Yang WW, Zhang WY, Qu ZG, He YL. Three-dimensional modeling of a PEMFC with serpentine flow field incorporating the impacts of electrode inhomogeneous compression deformation. Int J Hydrogen Energy 2019;44:22194–209. https://doi.org/10.1016/j.ijhydene.2019.06.187.
[145] Son J, Um S, Kim YB. Effect of stacking pressure on the performance of polymer electrolyte membrane fuel cell with various channel types. Energy Convers Manag 2021;232:113803. https://doi.org/10.1016/j.enconman.2020.113803.
[146] Kim S, Mench MM. Physical degradation of membrane electrode assemblies undergoing freeze/thaw cycling: micro-structure effects. J Power Sources 2007;174:206–20. https://doi.org/10.1016/j.jpowsour.2007.08.111.
[147] Netwall CJ, Gould BD, Rodgers JA, Nasello NJ, Swider-Lyons KE. Decreasing contact resistance in proton-exchange membrane fuel cells with metal bipolar plates. J Power Sources 2013. https://doi.org/10.1016/j.jpowsour.2012.11.012.
[148] Selamet OF, Ergoktas MS. Effects of bolt torque and contact resistance on the performance of the polymer electrolyte membrane electrolyzers. J Power Sources 2015. https://doi.org/10.1016/j.jpowsour.2015.01.162.

[149] Mason TJ, Millichamp J, Shearing PR, Brett DJL. A study of the effect of compression on the performance of polymer electrolyte fuel cells using electrochemical impedance spectroscopy and dimensional change analysis. Int J Hydrogen Energy 2013;38:7414–22. https://doi.org/10.1016/j.ijhydene.2013.04.021.

[150] Zhou P, Lin P, Wu CW, Li Z. Effect of nonuniformity of the contact pressure distribution on the electrical contact resistance in proton exchange membrane fuel cells. Int J Hydrogen Energy 2011;36:6039–44. https://doi.org/10.1016/j.ijhydene.2011.01.080.

[151] Avasarala B, Haldar P. Effect of surface roughness of composite bipolar plates on the contact resistance of a proton exchange membrane fuel cell. J Power Sources 2009. https://doi.org/10.1016/j.jpowsour.2008.11.063.

[152] Wang HC, Sheu HH, Lu CE, Hou KH, Ger M Der. Preparation of corrosion-resistant and conductive trivalent Cr-C coatings on 304 stainless steel for use as bipolar plates in proton exchange membrane fuel cells by electrodeposition. J Power Sources 2015. https://doi.org/10.1016/j.jpowsour.2015.05.105.

[153] Gago AS, Ansar SA, Saruhan B, Schulz U, Lettenmeier P, Canas NA, et al. Protective coatings on stainless steel bipolar plates for proton exchange membrane (PEM) electrolysers. J Power Sources 2016. https://doi.org/10.1016/j.jpowsour.2015.12.071.

[154] Turan C, Cora ON, Koç M. Investigation of the effects of process sequence on the contact resistance characteristics of coated metallic bipolar plates for polymer electrolyte membrane fuel cells. J Power Sources 2013. https://doi.org/10.1016/j.jpowsour.2013.05.182.

[155] Qiu D, Peng L, Yi P, Lai X. A micro contact model for electrical contact resistance prediction between roughness surface and carbon fiber paper. Int J Mech Sci 2017;124(125):37–47. https://doi.org/10.1016/j.ijmecsci.2017.02.026.

[156] Gauthier E, Duan Q, Hellstern T, Benziger J. Water flowin, through, and around the gas diffusion layer. Fuel Cell 2012. https://doi.org/10.1002/fuce.201100187.

[157] Simon C, Hasché F, Gasteiger HA. Influence of the gas diffusion layer compression on the oxygen transport in PEM fuel cells at high water saturation levels. J Electrochem Soc 2017. https://doi.org/10.1149/2.0691706jes.

[158] Jiao K, Li X. Water transport in polymer electrolyte membrane fuel cells. Prog Energy Combust Sci 2011;37:221–91. https://doi.org/10.1016/j.pecs.2010.06.002.

[159] Iranzo A, Boillat P. Liquid water distribution patterns featuring back-diffusion transport in a PEM fuel cell with neutron imaging. Int J Hydrogen Energy 2014. https://doi.org/10.1016/j.ijhydene.2014.08.042.

[160] Gao Y, Nguyen TV, Hussey DS, Jacobson D. In situ imaging of water distribution in a gas diffusion layer by neutron radiography. ECS Transactions 2019. https://doi.org/10.1149/1.3484635.

[161] Wang XR, Ma Y, Gao J, Li T, Jiang GZ, Sun ZY. Review on water management methods for proton exchange membrane fuel cells. Int J Hydrogen Energy 2020. https://doi.org/10.1016/j.ijhydene.2020.06.211.

[162] Esmaili Q, Nimvari ME, Jouybari NF, Chen YS. Model based water management diagnosis in polymer electrolyte membrane fuel cell. Int J Hydrogen Energy 2020;45:15618–29. https://doi.org/10.1016/j.ijhydene.2020.04.031.

[163] Kakaee AH, Molaeimanesh GR, Elyasi Garmaroudi MH. Impact of PTFE distribution across the GDL on the water droplet removal from a PEM fuel cell electrode containing binder. Int J Hydrogen Energy 2018;43:15481–91. https://doi.org/10.1016/j.ijhydene.2018.06.111.

[164] Chen T, Liu S, Zhang J, Tang M. Study on the characteristics of GDL with different PTFE content and its effect on the performance of PEMFC. Int J Heat Mass Tran 2019;128:1168–74. https://doi.org/10.1016/j.ijheatmasstransfer.2018.09.097.

[165] Mortazavi M, Santamaria AD, Chauhan V, Benner JZ, Heidari M, Médici EF. Effect of PEM fuel cell porous media compression on in-plane transport phenomena. Journal of Power Sources Advances 2020;1:100001. https://doi.org/10.1016/j.powera.2020.100001.

[166] Oztürk A, Fıçıcılar B, Eroğlu I, Bayrakçeken Yurtcan A. Facilitation of water management in low Pt loaded PEM fuel cell by creating hydrophobic microporous layer with PTFE, FEP and PDMS polymers: effect of polymer and carbon amounts. Int J Hydrogen Energy 2017;42:21226–49. https://doi.org/10.1016/j.ijhydene.2017.06.202.

[167] Chung S, Shin D, Choun M, Kim J, Yang S, Choi M, et al. Improved water management of Pt/C cathode modified by graphitized carbon nanofiber in proton exchange membrane fuel cell. J Power Sources 2018;399:350–6. https://doi.org/10.1016/j.jpowsour.2018.07.126.

[168] Ashrafi M, Shams M. The effects of flow-field orientation on water management in PEM fuel cells with serpentine channels. Appl Energy 2017;208:1083–96. https://doi.org/10.1016/j.apenergy.2017.09.044.

[169] Wu Y, Cho JIS, Neville TP, Meyer Q, Ziesche R, Boillat P, et al. Effect of serpentine flow-field design on the water management of polymer electrolyte fuel cells: an in-operando neutron radiography study. J Power Sources 2018;399:254–63. https://doi.org/10.1016/j.jpowsour.2018.07.085.

[170] Cha D, Ahn JH, Kim HS, Kim Y. Effects of clamping force on the water transport and performance of a PEM (proton electrolyte membrane) fuel cell with relative humidity and current density. Energy 2015;93:1338–44. https://doi.org/10.1016/j.energy.2015.10.045.

[171] Zhang C, Zhang L, Zhou W, Wang Y, Chan SH. Investigation of water transport and its effect on performance of higherature PEM fuel cells. Electrochim Acta 2014. https://doi.org/10.1016/j.electacta.2014.10.059.

[172] Dai W, Wang H, Yuan XZ, Martin JJ, Yang D, Qiao J, et al. A review on water balance in the membrane electrode assembly of proton exchange membrane fuel cells. Int J Hydrogen Energy 2009. https://doi.org/10.1016/j.ijhydene.2009.09.017.

[173] Ye X, Wang C-Y. Measurement of water transport properties through membrane-electrode assemblies. J Electrochem Soc 2007. https://doi.org/10.1149/1.2737379.

[174] Bazylak A, Sinton D, Liu ZS, Djilali N. Effect of compression on liquid water transport and microstructure of PEMFC gas diffusion layers. J Power Sources 2007;163:784–92. https://doi.org/10.1016/j.jpowsour.2006.09.045.

[175] Liu X, Peng F, Lou G, Wen Z. Liquid water transport characteristics of porous diffusion media in polymer electrolyte membrane fuel cells: a review. J Power Sources 2015;299:85–96. https://doi.org/10.1016/j.jpowsour.2015.08.092.

[176] Jiao K, Li X. Water transport in polymer electrolyte membrane fuel cells. Prog Energy Combust Sci 2011. https://doi.org/10.1016/j.pecs.2010.06.002.

[177] Zhan N, Wu W, Wang S. Pore network modeling of liquid water and oxygen transport through the porosity-graded bilayer gas diffusion layer of polymer electrolyte membrane fuel cells. Electrochim Acta 2019;306:264–76. https://doi.org/10.1016/j.electacta.2019.03.115.

[178] Lee WK, Ho CH, Van Zee JW, Murthy M. Effects of compression and gas diffusion layers on the performance of a PEM fuel cell. J Power Sources 1999;84:45–51. https://doi.org/10.1016/S0378-7753(99)00298-0.

[179] Khandelwal M, Mench MM. Direct measurement of through-plane thermal conductivity and contact resistance in fuel cell materials. J Power Sources 2006;161:1106–15. https://doi.org/10.1016/j.jpowsour.2006.06.092.

[180] Jouin M, Gouriveau R, Hissel D, Péra MC, Zerhouni N. Degradations analysis and aging modeling for health assessment and prognostics of PEMFC. Reliab Eng Syst Saf 2016;148:78–95. https://doi.org/10.1016/j.ress.2015.12.003.

[181] Zhao C, Xing S, Liu W, Chen M, Wang Y, Wang H. An experimental study on pressure distribution and performance of end-plate with different optimization parameters for air-cooled open-cathode LT-PEMFC. Int J Hydrogen Energy 2020;45:17902–15. https://doi.org/10.1016/j.ijhydene.2020.04.270.

[182] Barzegari MM, Ghadimi M, Momenifar M. Investigation of contact pressure distribution on gas diffusion layer of fuel cell with pneumatic endplate. Appl Energy 2020;263:114663. https://doi.org/10.1016/j.apenergy.2020.114663.

[183] Liu B, Liu LF, Wei MY, Wu CW. Vibration mode analysis of the proton exchange membrane fuel cell stack. J Power Sources 2016;331:299–307. https://doi.org/10.1016/j.jpowsour.2016.09.056.

[184] Liu B, Wei MY, Zhang W, Wu CW. Effect of impact acceleration on clamping force design of fuel cell stack. J Power Sources 2016;303:118–25. https://doi.org/10.1016/j.jpowsour.2015.10.061.

[185] Mikkola M, Tingelof T, Ihonen JK. Modelling compression pressure distribution in fuel cell stacks. J Power Sources 2009;193:269–75. https://doi.org/10.1016/j.jpowsour.2009.01.033.

[186] Zhou Z, Qiu D, Zhai S, Peng L, Lai X. Investigation of the assembly for high-power proton exchange membrane fuel cell stacks through an e ffi cient equivalent model. Appl Energy 2020;277:115532. https://doi.org/10.1016/j.apenergy.2020.115532.

[187] Montanini R, Squadrito G, Giacoppo G. Measurement of the clamping pressure distribution in polymer electrolyte fuel cells using piezoresistive sensor arrays and digital image correlation techniques. J Power Sources 2011;196:8484–93. https://doi.org/10.1016/j.jpowsour.2011.06.017.

[188] Ozden A, Shahgaldi S, Zhao J, Li X, Hamdullahpur F. Degradations in porous components of a proton exchange membrane fuel cell under freeze-thaw cycles: morphology and microstructure effects. Int J Hydrogen Energy 2020;45:3618–31. https://doi.org/10.1016/j.ijhydene.2018.10.209.

[189] Ozden A, Shahgaldi S, Li X, Hamdullahpur F. Degradations in the surface wettability and gas permeability characteristics of proton exchange membrane fuel cell electrodes under freeze-thaw cycles: effects of ionomer type. Int J Hydrogen Energy 2018. https://doi.org/10.1016/j.ijhydene.2018.11.184.

[190] Sadeghi Alavijeh A, Bhattacharya S, Thomas O, Chuy C, Yang Y, Zhang H, et al. Effect of hygral swelling and shrinkage on mechanical durability of fuel cell membranes. J Power Sources 2019;427:207–14. https://doi.org/10.1016/j.jpowsour.2019.04.081.

[191] Banan R, Bazylak A, Zu J. Combined effects of environmental vibrations and hygrothermal fatigue on mechanical damage in PEM fuel cells. Int J Hydrogen Energy 2015;40:1911–22. https://doi.org/10.1016/j.ijhydene.2014.11.125.

[192] Lin P, Zhou P, Wu CW. A high efficient assembly technique for large PEMFC stacks. Part I. Theory. J Power Sources 2009;194:381–90. https://doi.org/10.1016/j.jpowsour.2009.04.068.

[193] Lin P, Zhou P, Wu CW. A high efficient assembly technique for large proton exchange membrane fuel cell stacks: Part II. Applications. J Power Sources 2010;195:1383–92. https://doi.org/10.1016/j.jpowsour.2009.09.038.

[194] Al Shakhshir S, Cui X, Frensch S, Kær SK. In-situ experimental characterization of the clamping pressure effects on low temperature polymer electrolyte membrane electrolysis. Int J Hydrogen Energy 2017;42:21597–606. https://doi.org/10.1016/j.ijhydene.2017.07.059.

[195] Andreas-Schott B. US patent No.US 2008/0305380 A1. 2008.

[196] Andreas-Schott B. US patent No.US 2008/0311457 A1. 2008.

[197] Bogumil TD. US patent No.US 8012648 B2. 2011.

[198] Fu Y, Hou M, Yan X, Hou J, Luo X, Shao Z, et al. Research progress of aluminium alloy endplates for PEMFCs. J Power Sources 2007. https://doi.org/10.1016/j.jpowsour.2007.01.018.

[199] Liu D, Lai X, Ni J, Peng L, Lan S, Lin Z. Robust design of assembly parameters on membrane electrode assembly pressure distribution. J Power Sources 2007. https://doi.org/10.1016/j.jpowsour.2007.05.066.

[200] Xing XQ, Lum KW, Poh HJ, Wu YL. Optimization of assembly clamping pressure on performance of proton-exchange membrane fuel cells. J Power Sources 2010. https://doi.org/10.1016/j.jpowsour.2009.06.107.

[201] Taymaz I, Benli M. Numerical study of assembly pressure effect on the performance of proton exchange membrane fuel cell. Energy 2010;35:2134–40. https://doi.org/10.1016/j.energy.2010.01.032.
[202] Perng SW, Wu HW. A three-dimensional numerical investigation of trapezoid baffles effect on non-isothermal reactant transport and cell net power in a PEMFC. Appl Energy 2015. https://doi.org/10.1016/j.apenergy.2014.12.059.
[203] Kumar A, Reddy RG. Materials and design development for bipolar/end plates in fuel cells. J Power Sources 2004;129:62–7. https://doi.org/10.1016/j.jpowsour.2003.11.011.
[204] Yu HN, Kim SS, Suh J Do, Lee DG. Axiomatic design of the sandwich composite endplate for PEMFC in fuel cell vehicles. Compos Struct 2010;92:1504–11. https://doi.org/10.1016/j.compstruct.2009.10.026.
[205] Grot SA. US patent No.US 6428921 B1. 2002.
[206] Toshiyuki I. Google patent No.WO 2005/053080 A1. 2005.
[207] https://www.ballard.com/fuel-cell-solutions/fuel-cell-power-products/fuel-cell-stacks.
[208] https://www.powercell.se/en/products-and-services/fuel-cell-stacks.
[209] Boguslaw W. Google patent No.CA 2271706 C. 2003.
[210] Unoki S. US patent No.US 2011/0070520 A1. 2011.
[211] David M. Google patent No.WO 2016/205139 A1. 2016.
[212] Barton RH. US patent No.US 2013/0273452 A1. 2013.
[213] Wilson AR. US patent No.US 9806369 B2. 2017.
[214] Hood PD. US patent No.US 9774056 B2. 2017.
[215] Tanaka S. US patent No.US 2017/0025701 A1. 2017.
[216] Dave NT. US patent No.US 2005/0089737 A1. 2005.
[217] Mease KL. US patent No.US 6218039 B1. 2001.
[218] Allen JP. US patent No.US 6670069 B2. 2003.
[219] Steinbroner MP. US patent No.US 2006/0093890 A1. 2006.
[220] Ernst WD. US patent No.US 5945232. 1999.
[221] Wozniczka B. US patent No.US 5993987. 1990.
[222] Suh D-M. US patent No.US 2006/0240307 A1. 2006.
[223] Heo Y. US patent No.US 2014/0162168 A1. 2014.
[224] Chinnici AG. US patent No.US 2014/0255818 A1. 2014.
[225] Benjamin N. Peace. US patent No.US 7435501 B2. 2008.
[226] Narutoshi S. Google patent No.EP 0936689 B1. 2004.
[227] Jefferson. Google. Patent No.EP 1284521 A2. 2003.
[228] Carlstrom CM. US patent No.US 6200698 B1. 2001.
[229] Connor EJ. US patent No.US 2008/0145713 A1. 2008.
[230] Scott Blanchet. US patent No.US 6413665 B1. 2000.
[231] D'Aleo JM. US patent No.US 6372372 B1. 2002.
[232] Chen H, Pei P, Song M. Lifetime prediction and the economic lifetime of proton exchange membrane fuel cells. Appl Energy 2015;142:154–63. https://doi.org/10.1016/j.apenergy.2014.12.062.
[233] Porstmann S, Wannemacher T, Richter T. Overcoming the challenges for a mass manufacturing machine for the assembly of PEMFC stacks. Machines 2019;7. https://doi.org/10.3390/machines7040066.
[234] https://www.energy.gov/eere/fuelcells/doe-technical-targets-fuel-cell-systems-and-stacks-transportation-applications.
[235] Gurau V. Demonstration of an automated assembly process for proton exchange membrane fuel cells using robotic technology. ASEE Annual Conference and Exposition, Conference Proceedings 2014:24.359.1–24.359.7. https://doi.org/10.18260/1-2–20250.
[236] https://www.autoland-sachsen.com/skalierbarkeit-und-effizienz-im-visier/.
[237] Konold P, Muminovic A, Wehrheim M. Assembly of fuel cells and stacks with robots. Communications in Computer and Information Science 2009;33:168–79. CCIS.
[238] Gurau V, Armstrong-Koch T. Further improvements of an end-effector for robotic assembly of polymer electrolyte membrane fuel cells. Energies 2015;8:9452–63. https://doi.org/10.3390/en8099452.
[239] Laskowski C. Design-for-Manufacture guidelines for automated assembly of proton exchange membrane (PEM) fuel cell stacks. 2011.
[240] Laskowski C, Derby S. Fuel cell ASAP: two iterations of an automated stack assembly process and ramifications for fuel cell design-for-manufacture considerations. J Fuel Cell Sci Technol 2011;8. https://doi.org/10.1115/1.4000684.
[241] Boothroyd G. Product design for manufacture and assembly. Comput Aided Des 1994;26:505–20. https://doi.org/10.1016/0010-4485(94)90082-5.
[242] Williams M, Tignor K, Sigler L, Rajagopal C, Gurau V. Robotic arm for automated assembly of proton exchange membrane fuel cell stacks. J Fuel Cell Sci Technol 2014;11:1–5. https://doi.org/10.1115/1.4027392.
[243] Ahmad M, Ahmad B, Alkan B, Vera D, Harrison R, Meredith J, et al. Hydrogen fuel cell pick and place assembly systems: heuristic evaluation of reconfigurability and suitability. Procedia CIRP 2016;57:428–33. https://doi.org/10.1016/j.procir.2016.11.074.
[244] Isanaka SP, Sparks TE, Liou FF, Newkirk JW. Design strategy for reducing manufacturing and assembly complexity of air-breathing Proton Exchange Membrane Fuel Cells (PEMFC). J Manuf Syst 2016;38:165–71. https://doi.org/10.1016/j.jmsy.2015.10.004.
[245] Ahmad M, Alkan B, Ahmad B, Vera D, Harrison R, Meredith J, et al. The use of a complexity model to facilitate in the selection of a fuel cell assembly sequence. Procedia CIRP 2016;44:169–74. https://doi.org/10.1016/j.procir.2016.02.054.
[246] Bobka P, Gabriel F, Romer M, Engbers T, Willgeroth M, Droder K. Fast pick and place stacking system for thin, limp and inhomogeneous fuel cell components. Production at the Leading Edge of Technology 2019:389–99. https://doi.org/10.1007/978-3-662-60417-5_39.
[247] Bobka P, Gabriel F, Droder K. Fast and precise pick and place stacking of limp fuel cell components supported by artificial neural networks. CIRP Annals 2020;69:1–4. https://doi.org/10.1016/j.cirp.2020.04.103.
[248] Kimura Y, Oyama S, Giga A, Okonogi D. Development of new FC separator for Clarity fuel cell. Honda R&D Technical Review 2016;29:50–5.
[249] Nobuhiro S, Hideaki K, Yasuhiro N. New fuel cell stack for HONDA FCX clarity. Honda R&D Technical Review; 2009.
[250] http://www.alliedpower.tech/sc/advantage.php.
[251] Schafer J, Weinmann HW, Mayer D, Storz T, Hofmann J, Fleischer J. Synergien zwischen Batterie- und Brennstoffzelle. wt Werkstattstechnik online. 2020.